

Numb and Numbl are required for maintenance of cadherin-based adhesion and polarity of neural progenitors

Mladen-Roko Rašin¹, Valeswara-Rao Gazula¹, Joshua J Breunig¹, Kenneth Y Kwan¹, Matthew B Johnson¹, Susan Liu-Chen¹, Hua-Shun Li^{2,3}, Lily Yeh Jan², Yuh-Nung Jan², Pasko Rakic¹ & Nenad Sestan^{1,4}

The polarity and adhesion of radial glial cells (RGCs), which function as progenitors and migrational guides for neurons, are critical for morphogenesis of the cerebral cortex. These characteristics largely depend on cadherin-based adherens junctions, which anchor apical end-feet of adjacent RGCs to each other at the ventricular surface. Here, we show that mouse *numb* and *numb-like* are required for maintaining radial glial adherens junctions. *Numb* accumulates in the apical end-feet, where it localizes to adherens junction-associated vesicles and interacts with cadherins. *Numb* and *Numbl* inactivation in RGCs decreases proper basolateral insertion of cadherins and disrupts adherens junctions and polarity, leading to progenitor dispersion and disorganized cortical lamination. Conversely, overexpression of *Numb* prolongs RGC polarization, in a cadherin-dependent manner, beyond the normal neurogenic period. Thus, by regulating RGC adhesion and polarity, *Numb* and *Numbl* are required for the tissue architecture of neurogenic niches and the cerebral cortex.

RGCs are specialized neuroepithelial cells that are important in the development of the cerebral cortex, serving as both progenitors and migrational guides for neurons^{1–4}. RGCs are highly polarized, extending a short apical process that forms an end-foot attached to the ventricular zone (VZ) surface, and a longer basal (radial) process that guides migrating neurons³. The apical end-feet anchor adjacent RGCs to each other via cadherin-based adherens junctions to maintain their apical attachment and the neuroepithelial integrity of the VZ^{1–5}. The prototypical adherens junction is formed by homophilic interactions between classical cadherins, such as cadherin 1 (Cdh1) and cadherin 2 (Cdh2) (also known as E-cadherin and N-cadherin, respectively), which control adhesion by recruiting actin microfilaments via catenins^{6–9}. The adherens junctions and polarity of RGCs are maintained throughout the neurogenic period, at the end of which a controlled downregulation of polarity occurs^{3,10–13}. Some RGCs lose their adherens junctions and apical contacts and transform into multipolar parenchymal astrocytes^{3,10–13}. Other RGCs retract their basal process but retain adherens junctions to form the lining of the postnatal ventricles as ependymal cells. Thus, RGC intercellular contacts and polarity maintain the structural integrity of the VZ and growing cerebral wall. Consequently, abnormalities in RGC adhesion and polarity may underlie developmental brain disorders and tumor formation^{2,3,14}.

In this study, we present evidence that the maintenance of cadherin-based adherens junctions and polarity in mouse cortical RGCs requires

numb and *numb-like* (*Numbl*), homologs of the *Drosophila* endocytic adaptor protein *Numb*^{15–20}. *Numb* was originally identified as a cell fate determinant that segregates to the basal pole of *Drosophila* neural progenitors during asymmetric cell divisions, where it promotes neuronal cell fate in only one of two daughter cells by inhibiting Notch signaling^{15–17}. *Numb* regulates clathrin-dependent endocytosis of Notch by forming a complex with endocytic molecules Eps15 and AP-2 (refs. 17–19). However, *Numb* has also been implicated in the trafficking of other transmembrane proteins and in the development of dendrites, dendritic spines and axons^{21–24}. Recent studies of knockout mice show that *Numb* and *Numbl* are important in brain development^{25,26}. It has been proposed that in mice, unlike in *Drosophila*, *Numb* forms a crescent on the apical membrane of mitotic VZ progenitors during asymmetric division to inhibit Notch signaling and neuronal fate in the daughter cell that remains a progenitor^{20,26}. We show here that mitotic *Numb* localization is evolutionarily conserved, with predominant localization to the basolateral domain of mitotic RGCs in mice. The appearance of an apical *Numb* crescent in mitotic cells is caused by *Numb* being particularly enriched in the apical end-feet of adjacent interphase RGCs contacting mitotic RGCs. Furthermore, we show that in apical end-feet, *Numb* is colocalized with the cadherin-catenin adhesion complex and enriched in vesicular structures associated with adherens junctions. We also show that the phenotype associated with inactivation of *Numb* and *Numbl* in cortical

¹Department of Neurobiology, Yale University School of Medicine, 333 Cedar Street, New Haven, Connecticut 06510, USA. ²Howard Hughes Medical Institute, Departments of Physiology and Biochemistry, University of California San Francisco, 1550 4th Street, San Francisco, California 94143, USA. ³Developmental Neurobiology Program, Institute of Molecular Medicine and Genetics, Medical College of Georgia, 1120 15th Street, Augusta, Georgia 30912, USA. ⁴Correspondence should be addressed to N.S. (nenad.sestan@yale.edu).

Received 9 April; accepted 17 May; published online 24 June 2007; doi:10.1038/nn1924

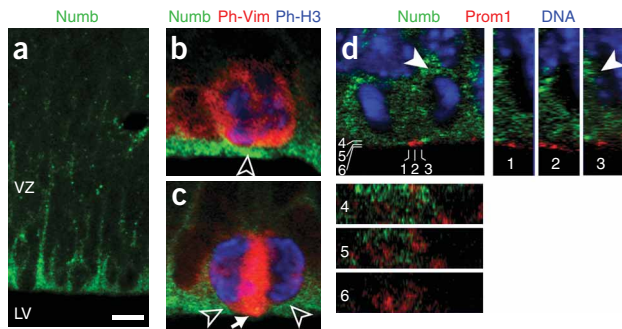


Figure 1 Numb is enriched in apical end-feet of interphase RGCs. (a–c) VZ cells in E16.5 dorsal telencephalon immunostained for Numb (green), Ph-Vim (red) and Ph-H3 (blue). Numb was enriched in apical end-feet of Ph-Vim[−]/Ph-H3[−] interphase cells (open arrowheads), but was mainly absent from the apical membrane of Ph-Vim⁺/Ph-H3⁺ mitotic cells (c, arrow). (d) Confocal z-stack image with orthogonal views (1–6) of E16.5 VZ surface immunostained for Numb (green) and Prom1 (red). Numb was localized in the basolateral cytoplasm of a dividing cell in late telophase (arrowhead), but was mainly excluded from the Prom1⁺ apical membrane. LV, lateral ventricle. Scale bar: 13 μ m in a, 3.5 μ m in b and c, 8 μ m in d.

RGCs cannot be explained solely by a loss of asymmetric cell divisions or activation of Notch signaling, but rather indicates a disruption of cadherin function. The present study reveals a role for Numb and Numbl in the maintenance of cadherin-mediated cell adhesion and polarity of RGCs and, consequently, the integrity of the VZ and cerebral cortex.

RESULTS

Numb is enriched in the apical end-feet of interphase RGCs

To analyze the function of Numb and Numbl in mouse cortical RGCs, we first examined their expression using *in situ* hybridization (ISH) and immunohistochemistry (IHC) during neurogenesis. ISH revealed that Numb and, to a lesser extent, Numbl were expressed by VZ cells (Supplementary Fig. 1 online), most of which coexpressed nestin and vimentin (Vim), markers of RGCs (data not shown). Because well-characterized antibodies to Numb are available, we conducted an examination of Numb protein localization. IHC confirmed previous observations²⁰ that most, if not all, VZ cells contain Numb, and that the most intense staining is present at the ventricular surface, with occasional unlabeled gaps (Fig. 1a and Supplementary Fig. 2 online). Previously, it was proposed that this intense immunostaining at the ventricular surface corresponds to a Numb protein crescent at the apical membrane of mitotic progenitor cells²⁰. However, when we carried out triple-labeled immunofluorescence staining at embryonic days 10.5 (E10.5), E13.5 and E16.5 for Numb, phosphorylated Vim (Ph-Vim, a cytoskeletal marker of mitotic RGCs) and phosphorylated histone 3 (Ph-H3, a nuclear marker of mitotic cells), we found that this intense Numb staining at the ventricular surface was present not within, but outside, the cell bodies of Ph-Vim and Ph-H3 double-positive mitotic cells, in what appeared to be the apical end-feet

of neighboring interphase RGCs (Fig. 1b,c; $n > 50$ cells at each stage). Furthermore, Numb immunolabeling was excluded from the prominin 1–positive (Prom1⁺) apical membrane²⁷ of mitotic progenitor cells, which probably accounts for the unlabeled gaps at the VZ surface (Fig. 1d). In Ph-Vim and Ph-H3 double-positive mitotic cells, Numb was detected throughout the basolateral compartment and in occasional basal processes. These results suggest that the intense Numb immunostaining at the ventricular surface during neurogenesis corresponds to the labeling of the apical end-feet of interphase RGCs surrounding mitotic RGCs, thus creating the artifactual appearance of a mitotic apical Numb crescent.

Numb localizes to adherens junction–associated vesicles

To confirm that Numb is enriched in apical end-feet and to examine its subcellular localization at the ventricular surface, we carried out pre-embedding immuno-electron microscopy using biotin- or gold-conjugated secondary antibodies (Fig. 2a–c and Supplementary Fig. 3 online; $n = 8$ brains). This analysis confirmed that intense Numb immunostaining corresponded to the apical end-feet of interphase RGCs, some of which surrounded mitotic cells (Fig. 2a,b). In the end-feet, Numb accumulated along the basolateral membrane and adherens junctions, as well as in numerous cytoplasmic vesicles (Fig. 2c; $n = 8$ brains), consistent with its proposed role as an endocytic adaptor protein^{17–19}. In contrast, Numb immunolabeling detected along the basolateral membrane and adherens junctions of mitotic cells was not as robust as it was in interphase end-feet (Fig. 2b,c). Furthermore, Numb immunolabeling was mainly excluded from the apical membrane of mitotic cells (Fig. 2a,b and Supplementary Fig. 3), which is consistent with the unlabeled gaps that we observed at the ventricular surface with immunofluorescence staining. Therefore, along the VZ surface, the highest concentration of Numb is in the thin apical end-feet of interphase cells, which surround the apical pole of the mitotic cell (illustrated in Fig. 2d,e). This localization of Numb mimics an apical crescent in the mitotic cell when examined under a light microscope.

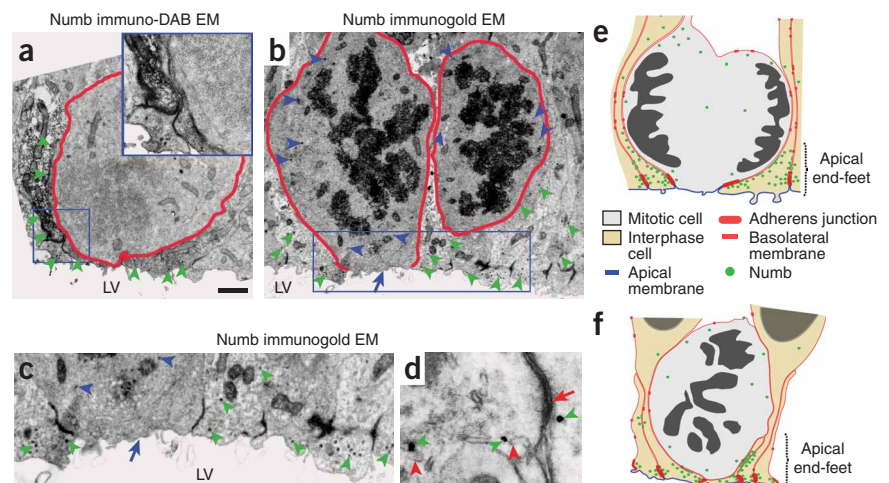


Figure 2 Numb localizes along the basolateral membrane and to vesicular structures near adherens junctions of interphase RGCs. (a–f) Electron microscopic (EM) analysis of Numb in E16.5 VZ using biotin- (a) or gold-conjugated (b–d) secondary antibodies. Numb (green arrowheads) was enriched along the apical-most end of the basolateral membrane (a,b, outlined in red), at adherens junctions (d, red arrow), and in associated cytoplasmic vesicles (d, red arrowheads) of interphase cells, as illustrated in e and f. In mitotic cells, Numb was present in the basolateral cytoplasm (blue arrowheads), but not at the apical membrane (b,c, blue arrow). Scale bar: 4 μ m in a and b, 1 μ m in d.

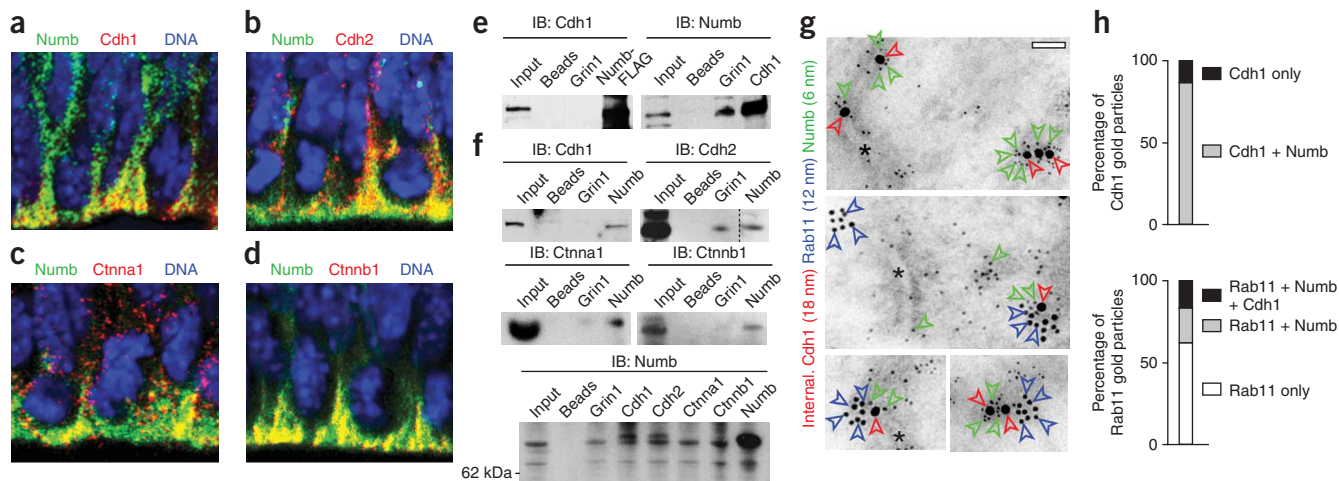


Figure 3 Numb colocalizes and interacts with cadherin-catenin adhesion complex. (a–d) Numb (green) colocalized in the apical end-feet of E16.5 RGCs with Cdh1 (a), Cdh2 (b), Ctnna1 (c) and Ctnnb1 (d), all red. (e) Flag-tagged Numb coimmunoprecipitated with Cdh1 and Grin1 in C6R radial glia-like cells. Cdh1 was precipitated with antibody to Flag, but not antibody to Grin1. (f) Numb coimmunoprecipitated with Cdh1, Cdh2, Ctnna1, Ctnnb1 and Grin1 in E16.5 dorsal forebrain. Dashed line indicates lane removed from the Cdh2 gel. IB, immunoblotting antibody. (g) Immunogold EM analysis showing association of Numb (green arrowheads) near adherens junctions (asterisks) with Rab11 (blue arrowheads) and internalized Cdh1 (red arrowheads), identified by 30-min internalization of antibody to Cdh1, in tissue slices of E16.5 neocortical wall. Scale bar: 50nm. (h) Quantification of gold particle associations in f.

Numb interacts with the cadherin-catenin complex in RGCs

The localization of Numb near adherens junctions motivated us to investigate a possible interaction between Numb and members of the cadherin-catenin adhesion complex, which are primary components of adherens junctions^{6–9}. We first carried out double-labeled immunofluorescence for Numb and members of the cadherin-catenin complex at E16.5 (Fig. 3a–d; $n = 3$). This analysis revealed that Numb was colocalized with Cdh1, Cdh2, catenin $\alpha 1$ (α (E)-catenin; Ctnna1) and catenin $\beta 1$ (β -catenin; Ctnnb1) in the apical end-feet of RGCs. Next, we carried out immunoprecipitation experiments to examine whether Numb and Numbl physically interact with members of the cadherin-catenin complex. We first tested this in cultured C6-R radial-like cells coexpressing Flag-tagged Numb or Numbl with human CDH1. We also used antibody to Grin1 as an immunoprecipitation control, because it precipitates Numb, but not Cdh1 (refs. 24,28). Antibodies to Cdh1 coprecipitated Flag-Numb and Flag-Numbl, but not Grin1, whereas in a complementary experiment, antibody to Flag precipitated CDH1 and, in the case of Flag-Numb, also Grin1 (Fig. 3e and Supplementary Fig. 4 online). Next we carried out immunoprecipitations with cell lysates from the E16.5 dorsal forebrain. Endogenous Numb coprecipitated with antibodies to Cdh1, Cdh2, Ctnna1, Ctnnb1 or Grin1 in the presence of either Nonidet P-40 or Triton X-100 detergents (Fig. 3f). Similarly, cadherins, catenins and Grin1 were coprecipitated with an antibody to Numb (Fig. 3f). These results show that Numb and Numbl interact with cadherins and catenins.

Numb associates with cadherin-containing endosomes

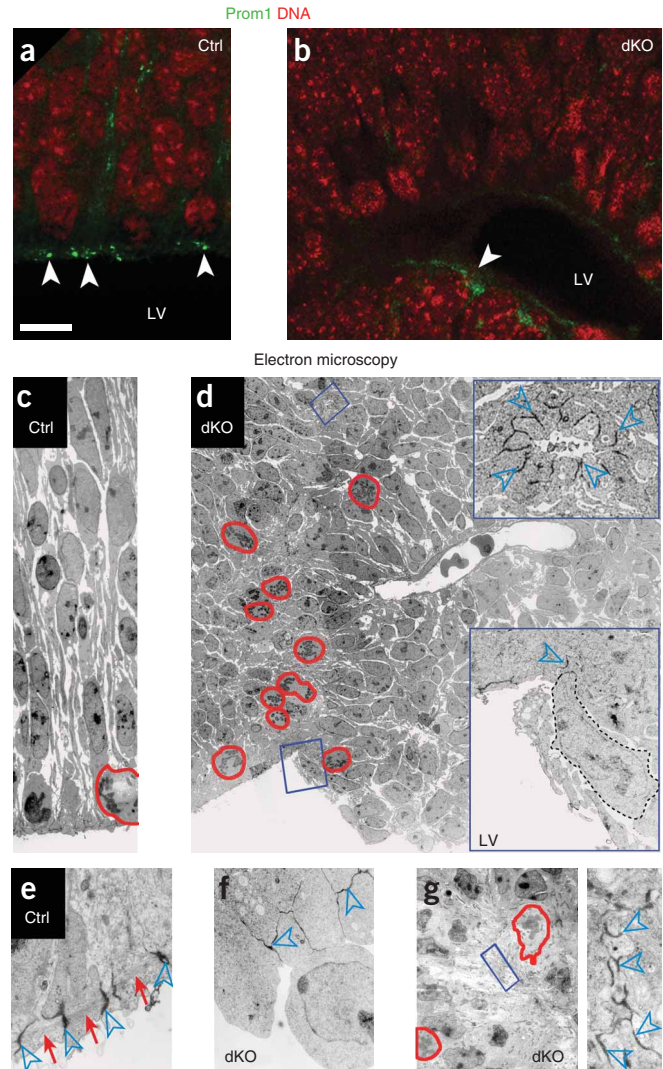
The establishment and maintenance of adherens junctions require proper targeting of cadherins from the trans-Golgi network to adherens junctions, as well as continuous internalization of cadherins and recycling to and from the cell surface via endosomes containing the GTPase Rab11 (refs. 29–31). Localization of Numb to the vesicular structures associated with adherens junctions and the basolateral membrane suggests that Numb may be involved in this process. Therefore, we assessed whether Numb associates with Rab11-positive recycling endosomes carrying Cdh1 in RGC apical end-feet. The

cycling pool of cell surface Cdh1 was labeled in cultured slices of E16.5 cerebral wall using a rat monoclonal antibody raised against the extracellular domain of mouse Cdh1, and a rat IgG was used as control treatment (Fig. 3g; $n = 10$ slices each). After an incubation period of 30 min, which allowed for the internalization and partial recycling of surface-bound antibodies, tissue slices were processed for postembedding triple-immunogold electron microscopy with antibodies against rat IgG, Rab11 and Numb. Under these conditions, 85.93 \pm 5.15% of gold particles labeling internalized Cdh1 at or near adherens junctions were surrounded by endogenous Numb, and 16.18 \pm 2.27% of Rab11 gold particles were associated with both Numb and Cdh1 particles (Fig. 3g). These data show that in the vicinity of adherens junctions, Numb associates with Cdh1 and Rab11⁺ recycling endosomes containing internalized Cdh1, components that are critical for the maintenance and remodeling of adherens junctions^{6–9,29–31}.

Disrupted VZ and ectopic progenitors in Numb and Numbl dKO

To determine whether *Numb* and *Numbl*, which have redundant functions during development^{25,26}, have a functional role in the maintenance of adherens junctions and cell adhesion, we used *Emx1*^{IRES-Cre} mice to inactivate *Numb* in the dorsal forebrain RGCs of *Numbl* null mice at the onset of neurogenesis²⁵. The *Numb* and *Numbl* double knockout mice (dKO, *Emx1*^{IRES-Cre/+}; *Numb*^{F/F}; *Numbl*^{−/−}) develop hydrocephalus perinatally and have severe cerebral cortical dysplasia (see also ref. 25). Embryos of control (*Emx1*^{IRES-Cre/+} or *Numb*^{F/F}; *Numbl*^{+/−}, $n \geq 2$ per stage) and dKO ($n \geq 2$ per stage) littermates at E10.5, E12.5, E16.5 and E18.5 were triple-immunostained for Vim, Cdh1 and Ph-H3, and counterstained with a nuclear DNA stain (Supplementary Fig. 5 online and data not shown). As reported previously²⁵, the neocortical VZ of E10.5 dKO embryos appeared to be columnar and pseudo-stratified, similar to control VZ, but was abnormally undulated (data not shown). However, during later embryonic development (E12.5–18.5), the dKO VZ epithelium transformed into a decreasingly columnar and increasingly disorganized VZ. Furthermore, the dKO VZ surface had multiple invaginations present in the cerebral wall, some of which resulted in rosette formations

Figure 4 Disruption of neuroepithelial integrity, adherens junctions and actin organization in *Numb* and *Numbl* dKO VZ. (**a,b**) Normal apical membrane localization of Prom1 (**a**, arrowheads) was lost in dKO embryos (**b**). Ctrl, control. (**c–g**) EM analysis of VZ at E12.5 (**c,d**) and E16.5 (**e–g**). The dKO VZ lacked columnar organization (**d** and lower inset, **f**) and many mitotic cells (red outlines) were detached from the surface (**d**). The remaining disorganized adherens junctions showed decreased electron density (blue arrowheads) with altered actin bundles (red arrows). Centers of rosettes contained mitotic cells and tangled adherens junctions (upper inset of **d**, **g** right). Scale bar: 11 μm in **a** and **b**, 10 μm in **c**, 28 μm in **d**, 6 μm in **e** and **f**, 20 μm in **g**.



that were composed of detached VZ cells. Vim immunostaining in the dKO revealed a significant disruption of RGC morphology and polarity (**Supplementary Fig. 5**), including the marked loss of Prom1 immunostaining at the VZ surface and its ectopic presence in both the neocortical wall and the center of rosettes (**Figs. 4a,b** and **5c**). Ph-H3–positive mitotic cells were ectopically distributed throughout the cerebral wall, in rosettes and in the lateral ventricles (**Supplementary Fig. 5**). The detachment and dispersion of RGCs was confirmed by the presence of ectopic Nestin-positive putative progenitors or immature Doublecortin-positive neurons in the late embryonic and postnatal neocortex of dKO animals (**Supplementary Figs. 6** and **7** online and data not shown). These results show that inactivation of *Numb* and *Numbl* disrupts the neuroepithelial organization of the VZ, causing RGCs to disperse.

Disrupted adherens junctions and RGC polarity in dKO

To examine whether adherens junctions and RGC polarity are affected in dKO embryos, we analyzed RGC ultrastructural organization using electron microscopy at E12.5 and E16.5. The VZ of control embryos ($n = 4$) was organized as a pseudo-stratified neuroepithelium. Mitotic cell bodies were localized to the ventricular (apical) surface, whereas elongated interphase cell bodies were located subjacent to the ventricular surface and maintained apical end-feet in close contact with neighboring cells (**Fig. 4c,d** and **Supplementary Fig. 8** online). Adherens junctions were localized near the ventricular surface and anchored to intracellular actin bundles (**Fig. 4d**). In the disorganized VZ of dKO littermates ($n = 3$), many cells lacked adherens junctions, polarized actin bundles and radial morphology, leading to the abnormal dispersion of mitotic cell bodies throughout the VZ and cerebral wall (**Fig. 4e–g** and **Supplementary Fig. 8**). Numerous multipolar cell bodies and fibers were abnormally present at the VZ surface and in the lateral ventricles of the dKO embryos (**Fig. 4e** and **Supplementary Fig. 8**). Furthermore, dKO embryos contained adherens junctions that were ectopically located at different levels of the VZ and within rosettes present in both the intermediate zone and cortical plate (**Fig. 4e,g** and **Supplementary Fig. 8**). These results demonstrate, at the ultrastructural level, that *Numb* and *Numbl* are required for the maintenance of adherens junctions and the neuroepithelial organization of the VZ. Notably, the cadherin-catenin adhesion complex is known to have a critical role in both of these processes^{2,5–8,32–35}.

Cadherins mislocalize in RGCs lacking *Numb* and *Numbl*

Because dKO mice have a brain phenotype consistent with an alteration of cadherin-mediated adhesion^{6,32–35}, we next examined whether the subcellular localizations of Cdh1 and Cdh2 are altered in dKO mice using immunogold electron microscopy in E12.5 and E16.5 embryos. In control embryos, Cdh1 and Cdh2 were primarily localized to the basolateral membrane and adherens junctions of RGCs, and were predominantly absent from the apical membrane (**Fig. 5**). In contrast, both Cdh1 and Cdh2 were widely distributed throughout the

cytoplasm of RGCs in dKO embryos (**Fig. 5b,d–h**). Furthermore, detailed analyses of dKO embryos revealed that Cdh1 was ectopically localized to the apical membrane (0.82 ± 0.64 of Cdh1-immunolabeled gold particles per μm of apical membrane at E12.5 and 2.88 ± 1.24 at E16.5 in dKO embryos, compared with 0.12 ± 0.26 at E12.5 and 0.07 ± 0.21 at E16.5 in Ctrl littermates; $P < 0.001$ for all) and throughout the Prom1⁺ central domain of rosettes, indicating its mislocalization to the apical membrane (**Fig. 5c,d–h**). Thus, in the absence of *Numb* and *Numbl*, the basolateral membrane localization and polarized distribution of cadherins in RGCs are markedly altered.

Cadherin shRNAs disrupt RGC adhesion and polarity

To determine whether the loss of *Cdh1* or *Cdh2* function would produce a phenotype similar to *Numb* and *Numbl* inactivation, we used *in utero* electroporation (IUE) to silence these genes with short hairpin RNAs (shRNAs). The ability of shRNAs to knock down gene expression was confirmed by both immunoblotting and immunostainings (**Supplementary Fig. 9** online). The pCGLH plasmids³⁶ (**Supplementary Fig. 9**) expressing shRNAs or negative control shRNAs, which contain point mutations or scrambled sequences with no homology to known mouse transcripts, were delivered into RGCs by IUE at E13.5 during the peak of neocortical neurogenesis ($n > 4$ animals for each condition).

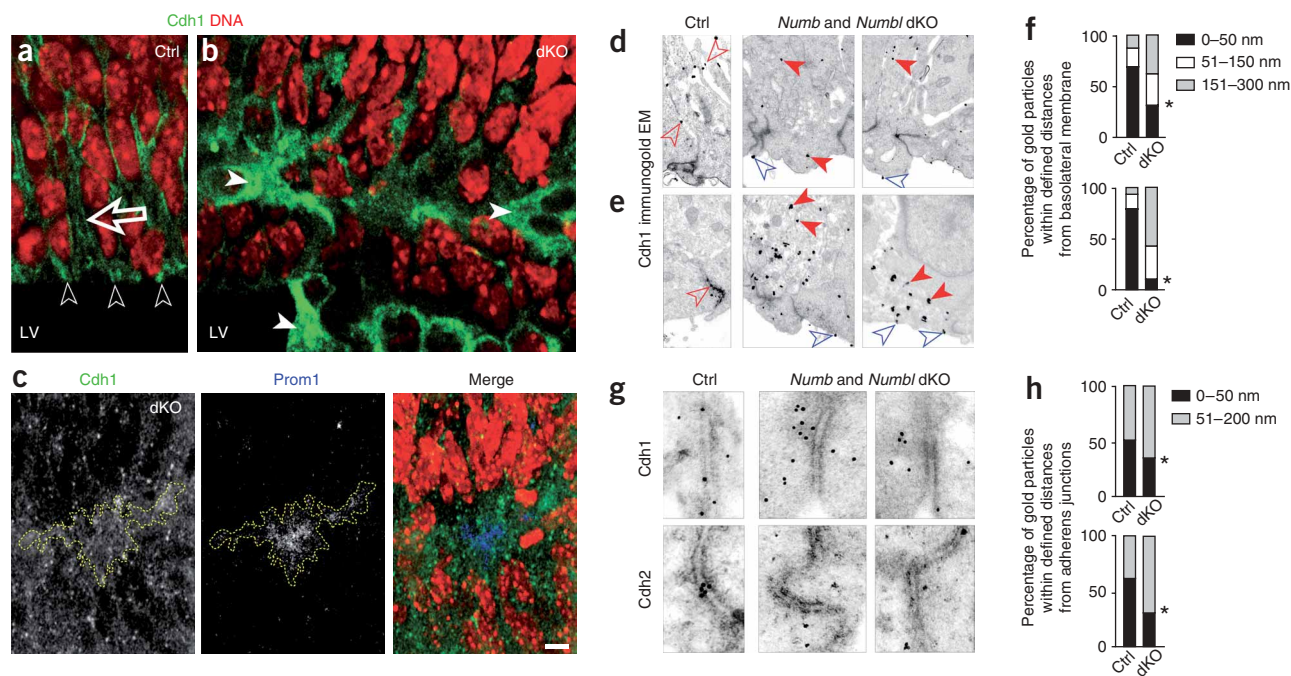


Figure 5 Altered subcellular localization of cadherins in *Numb* and *Numbl* dKO VZ. (a) Cdh1 (green) was localized to the basolateral membrane (arrow) and adherens junctions (open arrowheads) in controls (Ctrl). (b,c) In dKO VZ, Cdh1 accumulated in the cytoplasm (b, arrowheads) and ectopically in the Prom1⁺ (blue) rosette centers (c, yellow outline). (d,e) Immunogold analysis at E12.5 (d) and E16.5 (e) showed decreased basolateral (red arrowheads) and ectopic apical (blue arrowheads) membrane localization of Cdh1 in dKO. (f) Quantification of the proximity of gold particles to the basolateral membrane. (g) Immunogold analysis of Cdh1 (upper) and Cdh2 (bottom) at adherens junctions in control and dKO. (h) Quantification of the percentage of gold particles labeling either Cdh1 (upper) or Cdh2 (lower) within defined distances of adherens junctions. *P* < 0.005. Scale bar: 5 μm in a–c, 1 μm in d and e, 125 nm in g.

When analyzed at E16.5, GFP⁺ RGCs expressing negative control shRNAs showed typical bipolar morphology, with adherens junctions located around the apical end-feet contacting the VZ surface and long radial processes extending to the pial surface (Fig. 6a). In contrast, the majority of GFP⁺ RGCs coexpressing *Numb* and *Numbl* shRNAs lacked adherens junctions and showed partial loss of both bipolar morphology and apical end-feet at the ventricular surface (Fig. 6b). Similar to dKO embryos, GFP⁺ cell bodies were dispersed in the VZ and ectopically present in the lateral ventricles, indicating a disruption of VZ surface integrity. However, hydrocephalus or widespread cortical malformations were not observed in animals electroporated *in utero* with shRNA-expressing plasmids (*n* > 50 animals). At the ultrastructural level, the majority of these GFP⁺ cells lacked observable electron-dense adherens junctions (Fig. 6b), further corroborating a role for *Numb* and *Numbl* in the maintenance of adherens junctions. Similarly, GFP⁺ cells expressing *Cdh1* or *Cdh2* shRNAs lacked clear adherens junctions, showed a loss of end-feet and bipolar morphology, and were scattered (Fig. 6d,g). When human *CDH1* or *CDH2* were coexpressed with *Numb* and *Numbl* shRNAs, the majority of multipolar GFP⁺ cells lacked end-feet and adherens junctions in a manner similar to the neuroepithelial disorganization caused by silencing *Numb* and *Numbl*. This indicates that proper localization, rather than relative expression levels of cadherins, was disturbed (Fig. 6e,h). However, when plasmids expressing *Numbl*, *Cdh1* or *Cdh2* shRNAs were electroporated along with plasmids expressing full-length mouse *Numb*⁶⁵, human *CDH1* or human *CDH2*, respectively, the disruption of adherens junctions and neuroepithelial VZ organization was rescued, confirming the specificity of the shRNA constructs (Fig. 6c,f,i). These experiments demonstrate that either *Cdh1* or *Cdh2* inactivation can disrupt adherens junction maintenance and RGC polarity in a manner similar to the inactivation

of *Numb* and *Numbl*. Furthermore, increased levels of *CDH1* or *CDH2* are not sufficient to rescue the *Numb* and *Numbl* knockdown phenotype, indicating that *Numb* and *Numbl* are required for proper subcellular localization, rather than proper expression, of cadherins.

Numb-promoted RGC polarity and adhesion depend on cadherin

Because inactivation of *Numb* and *Numbl* or cadherins disrupted RGC adhesion and polarity, their forced expression may prolong the maintenance of RGC polarity beyond the end of neurogenesis. To test this hypothesis, we electroporated pCLEG plasmids³⁶ coexpressing GFP and one of the four previously reported *Numb* isoforms^{19,21}, *Numbl*, *CDH1* or *CDH2* at E16 (*n* ≥ 4 brains each) (Fig. 7 and Supplementary Fig. 10 online). When analyzed at postnatal day 10 (P10), GFP⁺ progenies of RGCs electroporated with the control pCLEG consisted of cells in the subependymal zone (SEZ) and pyramidal neurons in the upper cortical layers, which are generated at the end of the neurogenic period (Fig. 7a). Most GFP⁺ cells in the SEZ were located some distance away from the ventricular surface and showed a transitional morphology with short radial processes. In contrast, the majority of GFP⁺ cells in the SEZ overexpressing any of four *Numb* isoforms, *Numbl*, *CDH1* or *CDH2* remained attached to the ventricular surface (Fig. 7b–d and Supplementary Fig. 10). These GFP⁺/*Numb*⁺, GFP⁺/*Numbl*⁺, GFP⁺/*CDH1*⁺ and GFP⁺/*CDH2*⁺ cells showed an elongated radial morphology similar to that of embryonic RGCs, with a basal process spanning the thickness of the neocortex or extending deep into the striatal parenchyma. To confirm that this prolonged radial morphology is dependent on cadherins, we coelectroporated pCLEG plasmids coexpressing GFP and *Numb* with pCGLH plasmids expressing either *Cdh1* or *Cdh2* shRNA (Fig. 7e,f). In both cases, we observed a substantial depletion of fully polarized GFP⁺ RGCs showing elongated

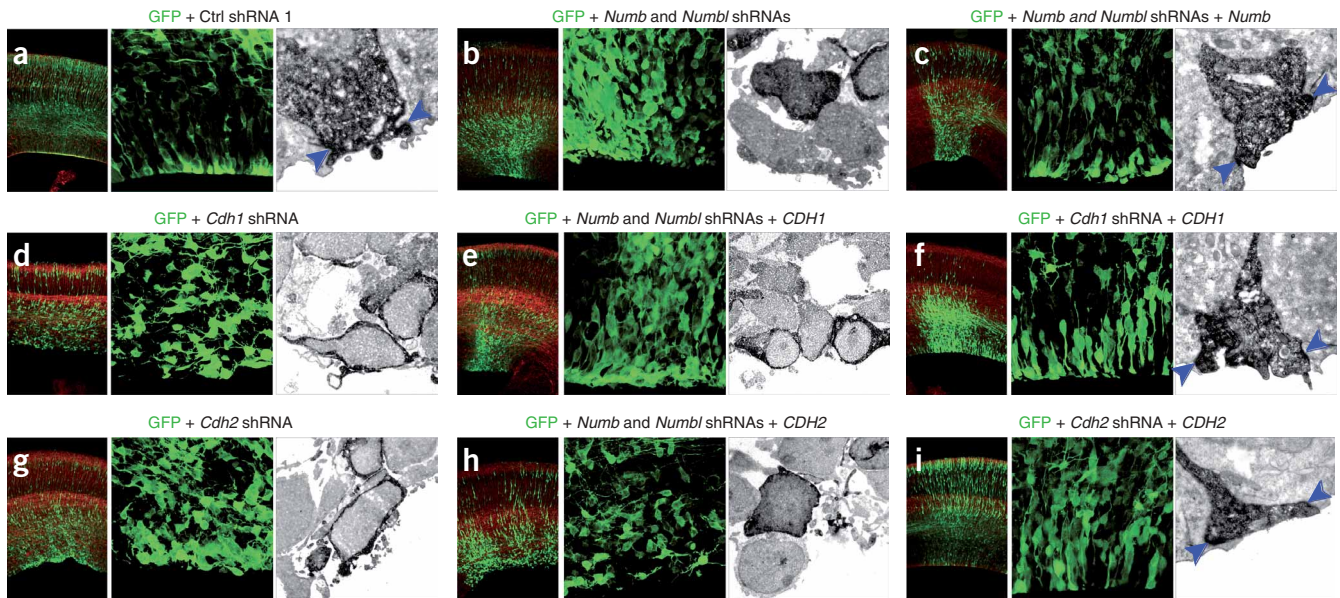


Figure 6 Loss of neuroepithelial integrity and adherens junctions in RGCs expressing *Numb* and *Numbl*, *Cdh1* or *Cdh2* shRNAs. (a–i) Confocal and immuno-DAB EM analyses of GFP⁺ E16.5 VZ cells (green) electroporated at E13.5 with pCGLH shRNA plasmids. Red stain is DNA. Cells expressing control shRNAs (a) or coexpressing corresponding overexpression constructs *Numb65* (c), *CDH1* (f) or *CDH2* (i) showed bipolar morphology with end-feet forming adherens junctions with surrounding cells at the ventricular surface (blue arrowheads in a,c,f,i). Disruption of radial morphology and adherens junctions, and detachment of apical processes in *Numb* and *Numbl* (b), *Cdh1* (d) and *Cdh2* (g) shRNA-expressing embryos. Disruption of the VZ was not rescued when *Numb* and *Numbl* shRNAs were coexpressed with *CDH1* or *CDH2* (e,h).

radial morphology and cell body attachment to the ventricular surface compared with that observed when *Numb* is overexpressed alone. Occasionally we observed GFP⁺ cells with a short radial-like process that did not reach the pial surface (Fig. 7e,f). These results indicate that forced expression of *Numb*, *Numbl*, *CDH1* or *CDH2* prolongs RGC polarity and increases anchoring to the ventricular surface. Moreover, these results show that *Numb*-mediated promotion of RGC polarity is dependant on cadherins.

RGC differentiation with altered *Numb* and *Numbl* expression

To examine whether *Numb*- and *Numbl*-mediated effects on RGC adhesion and polarity are associated with changes in neuronal and astrocytic differentiation, we first examined the differentiation of pyramidal neurons of early postnatal (P3, P10 and P21) dKO neocor-

tex, which showed disorganized lamination, axonal tracts and white matter (Fig. 8a and data not shown). Despite a severely malformed neocortex, several layer-specific pyramidal neuron markers (*Cutl1/Cux1* SMI-32, *Bcl11b/Ctip2*, *Foxp2*) were present in the dKO (Fig. 8a; $n = 3$), although with reduced abundance and density compared with control littermates ($n = 3$), indicating that both late- and early-born neurons are generated. Additional comparisons revealed that neurons in layers II–V were more severely affected than those in layer VI (Fig. 8a). Analysis of *Gfap* immunostaining showed no abnormal or premature astrocytic differentiation in dKO embryos (E16.5 and 18.5, $n = 2$ brains each; Supplementary Fig. 11 online and data not shown). However, a marked increase in the number of *Gfap*⁺ astrocytes was found in dKO mice throughout the neocortex and white matter during the early postnatal period,

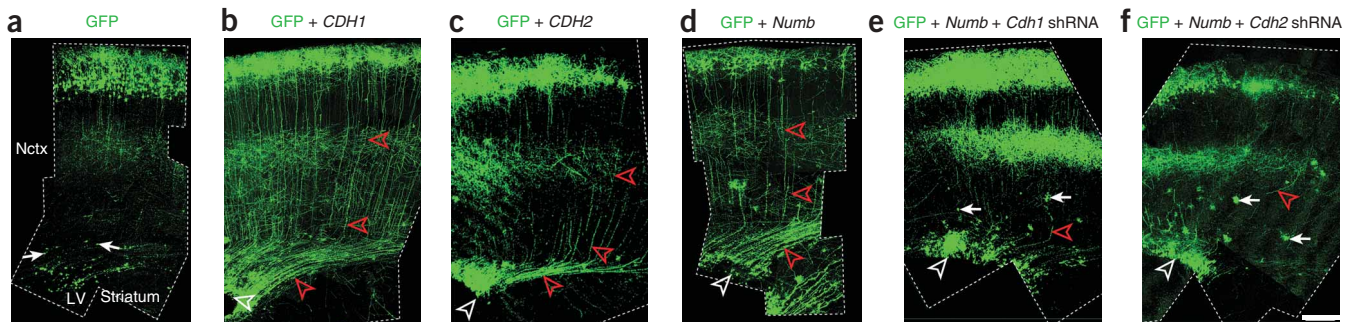


Figure 7 *Numb* and *Numbl* promote RGC polarity in a cadherin-dependent manner. (a–f) Confocal analysis of the corticostriatal junction of P10 brains electroporated at E16 with plasmids expressing GFP either alone (a) or in combination with *CDH1* (b), *CDH2* (c) or *Numb65* (d), or expressing *Numb65* in combination with either *Cdh1* (e) or *Cdh2* (f) shRNA. Most control GFP⁺ cells in the SEZ (a, arrows) had detached from the surface. *Numb65*-GFP⁺, *CDH1*-GFP⁺ and *CDH2*-GFP⁺ cells were present at the ventricular surface (b–d, white arrowheads) and showed long radial processes either spanning the neocortex (Nctx) (b–d, red arrowheads) or extending deep into the striatum. When *Cdh1* or *Cdh2* shRNA were coelectroporated with *Numb65*, GFP⁺ cells were found in the white matter (e,f, arrows); only a few GFP⁺ cells extended long radial processes, and these processes rarely spanned the entire Nctx (e,f, red arrowheads). Scale bar, 100 μ m.

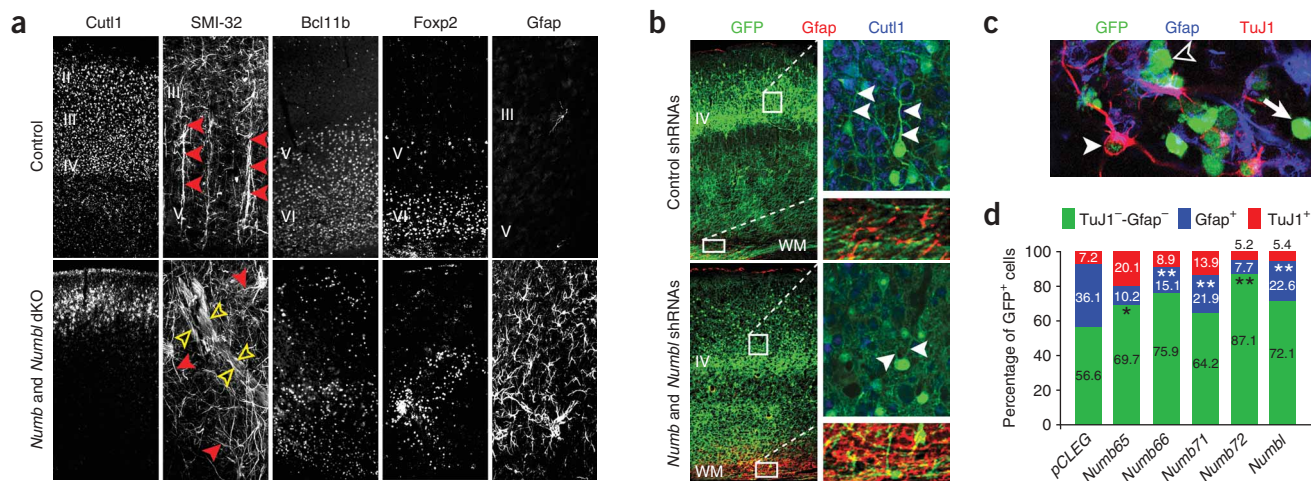


Figure 8 Effects of manipulating *Numb* and *Numbl* expression on the sequential generation of neocortical cell types. **(a)** Immunofluorescence staining of P21 mice for layer-specific pyramidal neuronal markers Cutl1 ($79 \pm 1\%$ density reduction in dKO as compared with control littermates, $P = 0.003$), Bcl11b ($73 \pm 5\%$ reduction, $P = 0.02$) and Foxp2 ($50 \pm 2\%$ reduction, $P = 0.02$). SMI-32 staining (layers V and III), revealed abnormal dendrites (red arrowheads) and axonal bundles (cyan arrowheads) of dKO neocortex (Nctx). A sixfold increase ($P = 0.02$) in the density of Gfap⁺ astrocytes in the dKO Nctx was observed. **(b)** Double immunostaining for Gfap (red) and Cutl1 (blue) in P14 mice electroporated at E13.5. GFP⁺ (green)-Cutl1⁺ superficial pyramidal neurons expressing *Numb* and *Numbl* shRNAs (green) were normally generated, but had disrupted dendrites (white arrowheads). Gfap (red) was not selectively increased in GFP⁺ *Numb* and *Numbl* shRNA-expressing cells. WM, white matter. **(c,d)** CLEG retroviral-mediated overexpression of one of four *Numb* isoforms or *Numbl* in cultured embryonic cortical progenitors (E13.5) moderately decreased astrocytic, but not neuronal, differentiation. **(c)** GFP⁺ progenies of infected progenitors were immunostained for Gfap (blue) and TuJ1 (red) 4 d after infection (**c**, green). Arrowhead indicates GFP⁺-TuJ1⁺ neuron (arrowhead), GFP⁺-Gfap⁺ astrocytes (open arrowhead) and GFP⁺-TuJ1⁻-Gfap⁻ cell (arrow), possibly representing an undifferentiated progenitor, could be identified. **(d)** Quantification of immunolabeled cells (* $P < 0.01$, ** $P \leq 0.001$, *** $P \leq 0.0001$).

subsequent to the development of severe hydrocephalus (**Fig. 8a** and data not shown).

Although these results do not exclude the possibility that *Numb* and *Numbl* have a role in the sequential differentiation of neurons and astrocytes, it is possible that at least some of the observed alterations are effects that are secondary to hydrocephalus, cortical malformations or Cre toxicity^{37–39}, rather than direct consequences of progenitor depletion or alteration in cell fate. Congenital hydrocephalus impairs cortical proliferation and increases cell death of progenitors and neurons, usually affecting late-born neurons more severely^{37–39}. To circumvent these possible secondary effects, we electroporated *Numb* and *Numbl* shRNA-expressing plasmids *in utero* at E13.5, when layer V pyramidal neurons are normally generated³⁶, and harvested tissue at P10 and P14 ($n > 2$ per condition per stage). At these ages, GFP⁺ pyramidal neurons were present in layers II–V, with no obvious laminar defects compared with control shRNAs (**Fig. 8b**). Furthermore, no substantial increase in astrocytic differentiation of GFP⁺ cells was observed in these animals (**Fig. 8b**). These results indicate that, in the absence of hydrocephalus, Cre expression and widespread cortical malformations, the silencing of *Numb* and *Numbl* by shRNAs does not disrupt the sequential generation of cortical neurons and astrocytes. Thus, it is likely that the loss of neuronal density and marked increase in astrocytic differentiation observed in dKO mice are secondary effects, possibly due to hydrocephalus. Although our shRNAs are able to knockdown *Numb* and *Numbl* gene expression substantially, the very small amount of residual *Numb* and *Numbl* proteins may be sufficient for the sequential generation of neurons, but be insufficient for maintenance of RGC adherens junctions and polarity.

To examine whether *Numb* overexpression affects the generation of neurons and astrocytes, we overexpressed *Numb* or *Numbl* in progenitors cultured from E13.5 neocortical wall, using the replication-defective CLEG retrovirus³⁶ ($n = 3$ separate infections of a 24-well

plate for each condition). The GFP⁺ progeny of infected progenitors expressing any one of the *Numb* isoforms or *Numbl* did not have significantly more class III β -tubulin (TuJ1)⁺ neurons 4 d after infection ($P > 0.05$). However, the same clones had a significantly smaller percentage of Gfap⁺ astrocytes ($P < 0.01$), indicating that either *Numb* or *Numbl* overexpression moderately diminishes astrocytic differentiation (**Fig. 8c,d** and data not shown). Collectively, these results indicate that neocortical neurogenesis and gliogenesis occur in normal sequential order despite the disruption of the neuroepithelial tissue architecture of the VZ.

DISCUSSION

The principal finding of this study is that *Numb* and *Numbl* are required for the maintenance of cadherin-mediated adhesion and polarity of RGCs during neocortical neurogenesis. This conclusion was drawn from several lines of evidence: predominantly, the localization of *Numb* to vesicular structures associated with adherens junctions, the molecular interaction of *Numb* with the cadherin-catenin adhesion complex and similarities between *Numb* and cadherin phenotypes. The localization of *Numb* to Rab11⁺-recycling endosomes containing internalized Cdh1 near adherens junctions is consistent with previous findings that *Numb* binds to the endocytic basolateral sorting motif and has a role in endosomal trafficking of transmembrane proteins^{18,19,21}. Loss of Rab11 function in epithelial cells leads to disrupted cell surface delivery of Cdh1, as well as to its abnormal placement on the apical membrane³⁰. Consistent with this phenotype, we show that in the absence of *Numb* and *Numbl*, cadherins were not properly localized to the basolateral membrane and adherens junctions, and in the case of Cdh1, they are mistargeted to the apical membrane. Furthermore, overexpression of either *CDH1* or *CDH2* was not sufficient to maintain the adhesion and polarity of RGCs when *Numb* and *Numbl* were silenced by shRNAs. Collectively, these results indicate that *Numb* and *Numbl* are required

for proper localization, rather than for proper expression, of cadherins to the basolateral membrane and adherens junctions.

We also show that *Numb* and *Numbl* inactivation causes a loss of adherens junctions, as well as RGC detachment and dispersion, comprising a phenotype consistent with the disruption of cadherin function^{6,32–35}. In contrast, forced expression of *Numb* or *Numbl* prolongs RGC apical attachment and polarization, and these effects are dependent on Cdh1 and Cdh2 function. Adhesion defects, consistent with the phenotype described here, also seem to be present in other *Numb* and *Numbl* dKOs. Recently, we have shown that adherens junctions are disrupted in the ependymal cells of mice with postnatal inactivation of *Numb* and *Numbl*²⁸. Additionally, the telencephalic neural tube of the Nestin-Cre dKO is misshapen, showing multiple folds consistent with disruption of VZ integrity²⁶. A later-stage cortical dKO generated using D6-cre has multiple rosette-like formations immunolabeled for the neural progenitor markers Neurogenin 2 and Musashi²⁶. Moreover, incorporation of BrdU by S-phase cells revealed disorganization of the pseudo-stratified VZ neuroepithelium²⁶, which is consistent with our findings. In addition, the loss of adherens junctions and RGC polarity occurs in mice lacking atypical PKC or Lgl1 (refs. 40,41), both of which regulate basolateral localization and Numb function⁴², further supporting Numb's role in cell adhesion. Together, these observations indicate that defects in adhesion and neuroepithelial organization of the VZ are present in all existing cortical *Numb* and *Numbl* dKO mice, as well as in other functionally related mice, but at different levels depending on the time of gene inactivation and the penetrance of Cre-mediated recombination. Because disturbances of Numb or cadherins have been linked to tumorigenesis^{7–9,43}, our results have important implications for brain tumors. Rosettes in the postnatal neocortex of dKO mice contain ectopic and likely neurogenic progenitors, central tangled junctional complexes and ectopic Prom1⁺ membrane (Fig. 4c and Supplementary Figs. 6 and 7), and closely resemble rosettes found in primitive neuroectodermal (neuroepithelial) human brain tumors^{44–46}.

Our results also clarify a number of discrepancies regarding the localization and function of Numb during mammalian neurogenesis. Our immunoelectron microscopic analysis showed that the previously reported apical Numb crescent in mitotic cells^{20,47} is likely a misinterpretation of intense immunolabeling in the thin apical end-feet of adjacent interphase cells, which surround the apical pole of the neighboring mitotic cells. During mitosis of RGCs, Numb is distributed throughout the cytoplasm of the basolateral domain. Together with previous reports in *Drosophila*^{15,16} and chick⁴⁸, our findings suggest that the localization of Numb to the basolateral compartment of mitotic neural progenitors is evolutionarily conserved.

Several lines of evidence strongly indicate that this newly described function for Numb in cell adhesion and polarity is independent of its previously described roles in the inhibition of Notch signaling and specification of cell fate during asymmetric cell division. First, Notch activation, which is expected to increase in the absence of Numb and *Numbl*, blocks cortical neurogenesis during embryogenesis without causing defects in RGC adhesion or polarity^{49,50} (data not shown). Consistent with this, expression of activated Notch in the postnatal ependymal and SEZ neural progenitor cells does not induce adhesion defects in the ependymal wall²⁸. Second, our results indicate that neither inactivation nor overexpression of Numb and *Numbl* blocks cortical neurogenesis in a manner similar to activated Notch. Moreover, in dKO mice, the astrocytic differentiation of RGCs lacking Numb and *Numbl* did not occur prematurely, but was increased during the perinatal period when cortical astrocytes are normally generated^{3,10–13}, and occurred after the appearance of hydrocephalus.

Furthermore, by using IUE to deliver shRNA-expressing plasmids after Cajal-Retzius neurons were generated, we have ruled out the possibility of secondary effects arising from the disruption of Cajal-Retzius neurons, which may indirectly affect RGC morphology and induce rosette formation as suggested previously²⁶. In conclusion, our study uncovers an additional function for Numb in regulating cell adhesion and polarity of neural progenitors, indicating that Numb has diverse roles in neural development.

METHODS

Immunohistochemistry and electron microscopy. Details on the procedure and the antibodies and dilutions used are shown in the **Supplementary Methods** and **Supplementary Table 1** online.

Immunoprecipitation and immunoblotting. E16.5 dorsal forebrain was lysed in 1% CHAPS lysis buffer (Pierce) containing protease inhibitors (Complete Mini, Roche Diagnostics), 1% Nonidet P-40 or 1% Triton X-100. C6-R cells were cotransfected with 5 µg of pFLAG-Numb65 and pCDH1 using the Amaxa Nucleofector system and processed 3 d later. Tissue or cells were homogenized with a high-speed homogenizer (Glas-Col) at 4 °C. Lysates were spun down for 30 min at 16,000g and supernatants were removed. Supernatants containing 500 µg of total protein were exposed for 1 h to protein A/G–Sepharose beads (Pierce Biotech) blocked with 20% BSA. These supernatants were then spun down to remove the Sepharose beads. Equal parts of the remaining supernatants were then exposed to rabbit anti-Numb (Upstate), goat anti-Numb (Novus Biologicals), rabbit anti-Grin1 (Chemicon), mouse anti-Cdh1 (Zymed), mouse anti-Cdh2 (Zymed), mouse anti-Ctnn1 (BD Transduction Laboratories), mouse anti-Ctnnb1 (BD Transduction Laboratories) or rabbit anti-Flag (Sigma) antibodies for 2 h rotating at 4 °C. New protein A/G–Sepharose beads also blocked with 20% BSA were added overnight. Precipitates were recovered by centrifugation, washed four times in PBS and two times in lysis buffer, and boiled for 10 min to release precipitates. We used 30 µg of proteins for immunoblotting. Blots were blocked using 5% fat-free milk in TBST for 1 h, and then exposed to corresponding primary antibodies for 1 h. After extensive washings, blotted protein was exposed to appropriate horseradish peroxidase-conjugated secondary antibodies and visualized with chemiluminescence systems (Chemiglow or Pierce Biotech). Details of antibodies and dilutions used are shown in **Supplementary Table 1**.

Internalization assay. Tissue slices of E16.5 forebrain (350 µm) were cut with the McIlwain tissue chopper and the Cdh1 internalization assay was carried out as described³¹ in HBSS medium supplemented with 0.5% glucose and 25 mM HEPES (Invitrogen) or in Neurobasal medium supplemented as described²². Briefly, slices were incubated with control rat IgG or rat antibody to extracellular Cdh1 (1:100; Zymed) diluted in medium for 1 h at 4 °C, and washed in ice-cold PBS. PBS was replaced with prewarmed medium and slices were incubated at 37 °C for 15 and 30 min. After washing in PBS and 0.5 M acetic acid to remove residual surface-bound antibodies, internalized antibodies were immunodetected by antibodies to rat IgG, Numb and Rab11 as described for postembedding immunogold electron microscopy in the **Supplementary Methods**.

In utero electroporation. Approximately 2 µl of DNA (4 µg µl⁻¹) were injected into the lateral ventricle and electroporated (five 50-ms pulses of 40 V at 950-ms intervals) as described³⁶. Details of plasmids and shRNA sequences are shown in **Supplementary Table 2** online.

Retroviral infection of cultured progenitors. The procedures for production of CLEG replication-defective retroviruses expressing all four Numb isoforms or *Numbl* are described in the **Supplementary Methods**. Dissociated cell cultures were prepared from E13.5 neocortical wall and plated at 25,000 cm⁻² onto polyornithine/laminin-coated glass coverslips in 24-well plates as described previously²². Retroviral supernatant (0.5–1 µl per well) was added to the cultures 2–4 h after plating. After 4 d, glass coverslips with cultured cells were gently washed with PBS, fixed with 4% PFA for 20 min and processed for double-labeled immunofluorescence staining with antibodies to neuronal class III β-tubulin (clone TuJ1) and Gfap. We collected 1-µm-thick optical sections with a 25× objective on a Zeiss LSM 510 confocal microscope.

Quantitative and statistical analysis. For postembedding electron microscopic analysis of E16.5 neocortical slices used for internalization assays, we quantified the association of immunogold particles for endogenous Numb and Rab11 with particles for internalized Cdh1 in 10 slices ($n > 700$ particles per each). For pre-embedding immunogold analysis of Cdh1 localization, the percentages of particles within 0–50 nm, 51–150 nm and 151–300 nm of the basolateral membranes of apical-end feet of control embryos or near the ventricular surface of dKO littermates were quantified ($n > 50$ ultrathin sections in each experiment), as was the density of particles 0–50 nm from apical membranes ($n > 50$ ultrathin sections in each experiment). For postembedding immunogold analysis of Cdh1 and Cdh2 localization in control and dKO embryos, the percentages of gold particles ($n > 700$ particles in each experiment) within 0–50 nm and 51–200 nm of adherens junctions were quantified. To quantitatively analyze the distribution of Cut1⁺, Bcl11b⁺, Foxp2⁺ and Gfap⁺ cells using the NeuroLucida system, tissue sections of the neocortex of control and dKO mice at P10 and P21 were stained using corresponding primary antibodies and counterstained with the DNA stain propidium iodide. The density and percentage of immunopositive cells were estimated by counting all immunopositive and propidium iodide-positive cells in the same volume of the neocortex from 2–4 nonconsecutive sections using the NeuroExplorer software. For retroviral infections of dissociated cultures, percentages of GFP⁺, TuJ1⁺ and Gfap⁺ cells were estimated on confocal optical sections ($n > 40$ per each infection). Data are presented as the mean \pm s.d. Student's *t*-tests were used for statistical comparisons.

Note: Supplementary information is available on the Nature Neuroscience website.

ACKNOWLEDGMENTS

We thank M. Pappy for experimental assistance, R. Flavell, M. Grumet, M. Inagaki, R. Medzhitov, J. Miyazaki, A. Nepveu, C. Gottardi, C. Walsh and W. Zhong for reagents, and M. Caplan, K. Herrup, J. LoTurco, A. Louvi and members of the Sestan lab for helpful discussions and comments. This study was supported by grants from the March of Dimes Birth Defects Foundation (FY05–73) and the US National Institutes of Health (HD045481, AG019394, NS047200). M.R.R. was supported by Autism Speaks. K.Y.K. was supported by the Canadian Institutes of Health Research. Y.N.J. and L.Y.J. are Investigators of the Howard Hughes Medical Institute.

COMPETING INTERESTS STATEMENT

The authors declare no competing financial interests.

Published online at <http://www.nature.com/natureneuroscience>

Reprints and permissions information is available online at <http://npg.nature.com/reprintsandpermissions>

- Fishell, G. & Kriegstein, A.R. Neurons from radial glia: the consequences of asymmetric inheritance. *Curr. Opin. Neurobiol.* **13**, 34–41 (2003).
- Götz, M. & Huttner, W.B. The cell biology of neurogenesis. *Nat. Rev. Mol. Cell Biol.* **6**, 777–788 (2005).
- Rakic, P. Developmental and evolutionary adaptations of cortical radial glia. *Cereb. Cortex* **13**, 541–549 (2003).
- Temple, S. The development of neural stem cells. *Nature* **414**, 112–117 (2001).
- Chenn, A. & McConnell, S.K. Intrinsic polarity of mammalian neuroepithelial cells. *Mol. Cell. Neurosci.* **11**, 183–193 (1998).
- Kadowaki, M. *et al.* N-cadherin mediates cortical organization in the mouse brain. *Dev. Biol.* **304**, 22–33 (2007).
- Perez-Moreno, M., Jamora, C. & Fuchs, E. Sticky business: orchestrating cellular signals at adherens junctions. *Cell* **112**, 535–548 (2003).
- Takeichi, M. The cadherin superfamily in neuronal connections and interactions. *Nat. Rev. Neurosci.* **8**, 11–20 (2007).
- Cavallaro, U. & Christofori, G. Cell adhesion and signalling by cadherins and IgCAMs in cancer. *Nat. Rev. Cancer* **4**, 118–132 (2004).
- Mission, J.P., Takahashi, T. & Caviness, V.S., Jr Ontogeny of radial and other astroglial cells in murine cerebral cortex. *Glia* **4**, 138–148 (1991).
- Schmid, R.S. *et al.* Neuregulin 1-erbB2 signaling is required for the establishment of radial glia and their transformation into astrocytes in cerebral cortex. *Proc. Natl. Acad. Sci. USA* **100**, 4251–4256 (2003).
- Smith, K.M. *et al.* Midline radial glia translocation and corpus callosum formation require Fgf signaling. *Nat. Neurosci.* **9**, 787–797 (2006).
- Alvarez-Buylla, A. & Lim, D.A. For the long run: maintaining germinal niches in the adult brain. *Neuron* **41**, 683–686 (2004).
- Taylor, M.D. *et al.* Radial glia cells are candidate stem cells of ependymoma. *Cancer Cell* **8**, 323–335 (2005).
- Doe, C.Q., Fuerstenberg, S. & Peng, C.Y. Neural stem cells: from fly to vertebrates. *J. Neurobiol.* **36**, 111–127 (1998).
- Jan, Y.N. & Jan, L.Y. Asymmetric cell division in the *Drosophila* nervous system. *Nat. Rev. Neurosci.* **2**, 772–779 (2001).
- Berdnik, D., Torok, T., Gonzalez-Gaitan, M. & Knoblich, J.A. The endocytic protein α -Adaptin is required for Numb-mediated asymmetric cell division in *Drosophila*. *Dev. Cell* **3**, 221–231 (2002).
- Santolini, E. *et al.* Numb is an endocytic protein. *J. Cell Biol.* **151**, 1345–1352 (2000).
- Smith, C.A., Dho, S.E., Donaldson, J., Teas, U. & McGlade, C.J. The cell fate determinant numb interacts with EHD/Rme-1 family proteins and has a role in endocytic recycling. *Mol. Biol. Cell* **15**, 3698–3708 (2004).
- Zhong, W., Feder, J.N., Jiang, M.M., Jan, L.Y. & Jan, Y.N. Asymmetric localization of a mammalian numb homolog during mouse cortical neurogenesis. *Neuron* **17**, 43–53 (1996).
- Roncarati, R. *et al.* The γ -secretase-generated intracellular domain of β -amyloid precursor protein binds Numb and inhibits Notch signaling. *Proc. Natl. Acad. Sci. USA* **99**, 7102–7107 (2002).
- Sestan, N., Artavanis-Tsakonas, S. & Rakic, P. Notch signaling mediates contact-dependent inhibition of cortical neurite growth. *Science* **286**, 741–746 (1999).
- Huang, E.J. *et al.* Targeted deletion of numb and numblike in sensory neurons reveals their essential functions in axon arborization. *Genes Dev.* **19**, 138–151 (2005).
- Nishimura, T. *et al.* Role of numb in dendritic spine development with a Cdc42 GEF intersectin and EphB2. *Mol. Biol. Cell* **17**, 1273–1285 (2006).
- Li, H.S. *et al.* Inactivation of Numb and Numbl like in embryonic dorsal forebrain impairs neurogenesis and disrupts cortical morphogenesis. *Neuron* **40**, 1105–1118 (2003).
- Petersen, P.H., Zou, K., Krauss, S. & Zhong, W. Continuing role for mouse Numb and Numbl in maintaining progenitor cells during cortical neurogenesis. *Nat. Neurosci.* **7**, 803–811 (2004).
- Kosodo, Y. *et al.* Asymmetric distribution of the apical plasma membrane during neurogenic divisions of mammalian neuroepithelial cells. *EMBO J.* **23**, 2314–2324 (2004).
- Kuo, C.T. *et al.* Postnatal deletion of Numb/Numbl like reveals repair and remodeling capacity in the subventricular neurogenic niche. *Cell* **127**, 1253–1264 (2006).
- Bryant, D.M. & Stow, J.L. The ins and outs of E-cadherin trafficking. *Trends Cell Biol.* **14**, 427–434 (2004).
- Lock, J.G. & Stow, J.L. Rab11 in recycling endosomes regulates the sorting and basolateral transport of E-cadherin. *Mol. Biol. Cell* **16**, 1744–1755 (2005).
- Paterson, A.D., Parton, R.G., Ferguson, C., Stow, J.L. & Yap, A.S. Characterization of E-cadherin endocytosis in isolated MCF-7 and Chinese hamster ovary cells: the initial fate of unbound E-cadherin. *J. Biol. Chem.* **278**, 21050–21057 (2003).
- Lien, W.H., Klezovitch, O., Fernandez, T.E., Delrow, J. & Vasioukhin, V. α E-Catenin controls cerebral cortical size by regulating the Hedgehog signaling pathway. *Science* **311**, 1609–1612 (2006).
- Ganzler-Odenthal, S.I. & Redies, C. Blocking N-cadherin function disrupts the epithelial structure of differentiating neural tissue in the embryonic chicken brain. *J. Neurosci.* **18**, 5415–5425 (1998).
- Machon, O., van den Bout, C.J., Backman, M., Kemler, R. & Krauss, S. Role of β -catenin in the developing cortical and hippocampal neuroepithelium. *Neuroscience* **122**, 129–143 (2003).
- Masai, I. *et al.* N-cadherin mediates retinal lamination, maintenance of forebrain compartments and patterning of retinal neurites. *Development* **130**, 2479–2494 (2003).
- Chen, J.G., Rasin, M.R., Kwan, K.Y. & Sestan, N. Zfp312 is required for subcortical axonal projections and dendritic morphology of deep-layer pyramidal neurons of the cerebral cortex. *Proc. Natl. Acad. Sci. USA* **102**, 17792–17797 (2005).
- Mashayekhi, F. *et al.* Deficient cortical development in the hydrocephalic Texas (H-Tx) rat: a role for CSF. *Brain* **125**, 1859–1874 (2002).
- Khan, O.H., Enno, T.L. & Del Bigio, M.R. Brain damage in neonatal rats following kaolin induction of hydrocephalus. *Exp. Neurol.* **200**, 311–320 (2006).
- Forni, P.E. *et al.* High levels of Cre expression in neuronal progenitors cause defects in brain development leading to microencephaly and hydrocephaly. *J. Neurosci.* **26**, 9593–9602 (2006).
- Imai, F. *et al.* Inactivation of aPKC lambda results in the loss of adherens junctions in neuroepithelial cells without affecting neurogenesis in mouse neocortex. *Development* **133**, 1735–1744 (2006).
- Klezovitch, O., Fernandez, T.E., Tapscott, S.J. & Vasioukhin, V. Loss of cell polarity causes severe brain dysplasia in Lgl1 knockout mice. *Genes Dev.* **18**, 559–571 (2004).
- Smith, C.A. *et al.* aPKC-mediated phosphorylation regulates asymmetric membrane localization of the cell fate determinant Numb. *EMBO J.* **26**, 468–480 (2007).
- Pece, S. *et al.* Loss of negative regulation by Numb over Notch is relevant to human breast carcinogenesis. *J. Cell Biol.* **167**, 215–221 (2004).
- Singh, S.K. *et al.* Identification of human brain tumour initiating cells. *Nature* **432**, 396–401 (2004).
- Langford, L.A. The ultrastructure of the ependymoblastoma. *Acta Neuropathol. (Berl.)* **71**, 136–141 (1986).
- Osana, M., Yamaguchi, J., Kikuchi, K., Satoh, M. & Sawada, N. Unique cellular features of peripheral primitive neuroectodermal tumor: ultrastructural evidence of its unique cytodifferentiation. *Med. Electron Microsc.* **37**, 193–197 (2004).
- Cayouette, M. & Raff, M. Asymmetric segregation of Numb: a mechanism for neural specification from *Drosophila* to mammals. *Nat. Neurosci.* **5**, 1265–1269 (2002).
- Wakamatsu, Y., Maynard, T.M., Jones, S.U. & Weston, J.A. NUMB localizes in the basal cortex of mitotic avian neuroepithelial cells and modulates neuronal differentiation by binding to NOTCH-1. *Neuron* **23**, 71–81 (1999).
- Gaiano, N. & Fishell, G. The role of Notch in promoting glial and neural stem cell fates. *Annu. Rev. Neurosci.* **25**, 471–490 (2002).
- Yang, X. *et al.* Notch activation induces apoptosis in neural progenitor cells through a p53-dependent pathway. *Dev. Biol.* **269**, 81–94 (2004).



Supplementary methods

Numb and Numbl are required for maintenance of cadherin–based adhesion and polarity of neural progenitors

Mladen-Roko Rašin, Valeswara-Rao Gazula, Joshua J. Breunig, Kenneth Y. Kwan, Matthew B. Johnson, Susan Liu-Chen, Hua-Shun Li, Lily Yeh Jan, Yuh-Nung Jan, Pasko Rakic, and Nenad Šestan

Animals. Experiments were carried out with CD-1 mice in accordance with a protocol approved by the Committee on Animal Research at Yale University. Generation of *Numb* and *Numbl* dKO mice was reported previously^{S1}. The morning of a detectable vaginal plug and the first neonatal day were considered to be embryonic day 0.5 (E0.5) and postnatal day 0 (P0), respectively.

Immunohistochemistry and light microscopy. For immunohistochemistry, brain tissue was fixed with 4% paraformaldehyde (PFA), pH 7.4 in PBS overnight. After washings in PBS, tissue was cryoprotected in graded sucrose solutions (10%, 20% and 30%) at 4°C, embedded in Tissue-Tek O.C.T. compound (Sakura Finetek), frozen at –40°C in 2-methylbutane and stored at –80°C. Frozen sections (40 µm) were incubated in blocking solution (BS) containing 5% normal donkey serum (Jackson ImmunoResearch Laboratories), 1% bovine serum albumin, 0.1% glycine, 0.1% L-lysine, and 0.3% Triton X-100 in PBS for 1 hr at room temperature (RT). Tissue sections were then incubated for two nights at 4°C in primary antibodies diluted in BS. After washing in PBS, tissue was incubated with appropriate donkey FITC-, Cy2-, Cy3-, or Cy5-conjugated secondary antibodies (1:250; Jackson ImmunoResearch Laboratories) for 2 hr at RT. Sections were washed in PBS and counterstained with DNA stains as described below. Single optical and z-stack images were collected on a Zeiss LSM 510 laser-scanning microscope or Zeiss Axioplan 2. For light immunohistochemistry on cultured dissociated cells, cells were fixed for 15 min in warm 4% PFA, BS, primary, and appropriate secondary antibodies were applied for 1 hr each, with PBS washes between each step and processed for immunofluorescence as described above. Details on the antibodies and dilutions used are shown in Supplementary Table 1.

Plasmid construction and cloning. For RNA interference, a template for shRNA synthesis was made by annealing two pairs of oligonucleotides representing sense and antisense strands of the target sequence. The annealed template was cloned into the BglII and SalI sites of pCGLH, a shRNA plasmid co-expressing GFP^{S2}. Negative control shRNAs were designed by mutating three nucleotides in the corresponding shRNA sequences. In addition, four scrambled oligonucleotide sequences were also used as negative controls. For overexpression, cDNAs were cloned into the pCLEG vector that co-expresses GFP, as described^{S2}. For overexpression experiments, the full-length mouse *Numb65*, *Numb66*, *Numb71*, *Numb72*, and *Numbl* were subcloned into pCLEG^{S3}. Empty pCLEG was used as the control. All overexpression vectors were co-electroporated with pCAGGS-GFP (4:1, pCLEG:pCAGGS-GFP). Details of plasmids and shRNA sequences are included in Supplementary Table 2.

In utero electroporation. For RNAi, embryos were electroporated at E13.5 with shRNA plasmids or control plasmids, and analyzed at E16.5, E18.5, P10, or P14. *Numb* and *Numbl* shRNA-expressing plasmids were combined at a ratio of 3:2. For overexpression, embryos were transfected at E16 and analyzed at P7 or P10. For co-electroporation of shRNAs and adequate overexpression, vectors (8 $\mu\text{g}/\mu\text{l}$) were mixed at a ratio of 1:1 so that the final concentration was the same as in single plasmid injections.

Electron microscopy. For regular electron microscopy (EM), brains were fixed in 4% PFA with 2% glutaraldehyde in PB (six changes of fixative every 30 min at RT and then overnight at 4°C). Tissue was sectioned on a vibratome at 70 μm and post-fixed in 1% OsO₄ for 45 min at RT and dehydrated as follows: 2x1 min in 50% EtOH, 45 min in 1% uranyl acetate in 70% EtOH, 2x1 min each in 70%, 90% and 100% EtOH and in propylene oxide. Sections were then embedded overnight in Durcupan (Sigma-Aldrich), mounted on microscopy slides, and kept at 60°C overnight. The VZ was identified by light microscopy and was re-embedded, cut ultra-thin (60 nm), collected on single whole copper grids (Electron Microscopy Sciences), and contrasted with lead-citrate for 2-4 min before EM analysis. All EM images were captured with the Multiscan 792 digital camera (Gatan, Pleasanton, CA).

Immuno-electron microscopy. For pre-embedding immuno-electron microscopy (immuno-EM), brain tissue was fixed in 4% PFA with 0.3% glutaraldehyde and sectioned on a vibratome at 70 μm . Sections were preincubated in blocking solution (BS) containing 5% normal donkey serum (Jackson ImmunoResearch Laboratories), 1% bovine serum albumin, 0.1% glycine and 0.1% L-lysine and then incubated with primary antibodies/BS for 36 hrs. For DAB immuno-EM, biotinylated secondary antibodies were applied for 2 hr followed by the avidin peroxidase complex (ABC Elite, Vector Labs). Reactions were visualized with 0.05% 3, 3'-diaminobenzidine, 0.04% ammonium chloride, 0.5-1mg glucose oxidase type VII, and 80 μl of 0.05M nickel ammonium sulfate in 0.2M acetate buffer (pH 6.0). The peroxidase reaction was started by adding 400 μl of 10% (w/v) 10% D-glucose in dH_2O and stopped 5-10 min later by washing in PBS. For pre-embedding immunogold EM, primary antibodies were applied as above. After washings, tissue and sections were incubated in BS with 0.1% gelatin (Amersham) for 1 hr. Secondary antibodies conjugated to 1 nm or 10 nm gold particles (Amersham) were applied overnight at 4°C. After washings and 10 min fixation in 1% glutaraldehyde (Electron Microscopy Sciences), and additional washings in PBS and dH_2O , silver intensification was applied as recommended by the manufacturer (Aurion). After DAB and gold immunostainings, sections were dehydrated as described above.

For post-embedding immunogold EM staining of 350 μm thick cultured slices used for internalization assay, slices were fixed as described above for 3 hr. For post-embedding immunogold EM staining of E12.5 neocortical wall brains were fixed and sectioned (70 μm thick) as described above. Then, tissue slices and sections were dehydrated for 20 min in both 50% and 70% ethanol at 4°C and incubated for 30 min at -20°C in 90% EtOH. Further 2 hr steps were done at -20°C in different embedding solutions of 50% EtOH and 50% LR Gold (SPI supplies), 30% EtOH and 70% LR Gold and twice in 100% LR Gold. After that, slices and sections were placed into the solution of 0.3% benzyl (SPI Supplies) in pure LR Gold overnight, and then transferred to gelatin capsules in 0.3% benzyl in LR Gold at -20°C and exposed to UV radiation for approximately 36 hr until LR Gold hardened. Ultrathin sections (70 nm) were collected on formvar-coated nickel mesh grids (Electron Microscopy Sciences). After washings, grids containing sections were washed six times in PBS at RT and blocked for 30 min with BS that contained 5% normal donkey serum, 1% bovine serum albumin, 0.2% glycine, 0.2% lysine and 2% fish skin gelatin. Grids were then exposed for one hour to goat anti-Numb and rabbit anti-Rab11 primary antibodies. Afterwards, grids were incubated for one hour with donkey anti-goat (6 nm), anti-rabbit (12 nm), and anti-rat (18 nm) (Jackson

ImmunoResearch; 1:40 in BS) gold conjugated secondary antibodies. After washings, 10 min fixation in 2% glutaraldehyde and additional washes in dH₂O, grids were air-dried. Immunogold stained sections were then contrasted with 2% uranyl acetate for 35 min before examination with the electron microscope. Negative controls included stainings with no primary antibody or with species-mismatched secondary antibodies.

***In situ* hybridization.** *In situ* hybridization histochemistry was performed as previously described^{S1}, using riboprobes corresponding to mouse *Numb* and *Numbl*^{S4,S5}.

DNA Stains. TOPRO was applied according to manufacturer's instructions (1:1000; Molecular Probes). DAPI was applied for 10 min (1:1000; Molecular Probes) and propidium iodide was applied for 5 min (10 mg/ml) at RT.

RNA interference. To test RNA interference efficiency, N2a cells were grown to 80% confluence in 10 cm dishes and transfected with 5 µg of shRNA-expressing plasmids using the Amaxa Nucleofector system (Amaxa) or Lipofectamine2000 (Invitrogen) according to the manufacturer's protocol. Three days later, GFP⁺ cells were collected by FACS, lysed on ice in CHAPS extraction buffer containing protease inhibitor (Roche) and 1% Nonidet P40 (NP40; Fluka), homogenized, and centrifuged. Forty µg of total protein was used for Western blotting. Blots were incubated with one of the following: rabbit anti-Numb^{S4}, rabbit anti-Numbl (Proteintech Group), mouse anti-Cdh1 (BD Transduction Laboratories), mouse anti-Cdh2 (Zymed), or rabbit anti-GFP (Molecular Probes). Peroxidase-coupled secondary antibodies (Jackson ImmunoResearch Laboratories) and the enhanced chemiluminescence system (Pierce Biotech) were used to visualize the blotted proteins. No signal for Cdh2 was detected in N2a cells expressing either control or Cdh1 shRNAs (data not shown).

Immunoprecipitation assays and immunoblotting. C6-R radial glia-like cells were co-transfected with 5 µg of pFLAG-Numb or pFLAG-Numbl^{S3} and 5 µg of pCDH1 using the Amaxa Nucleofector system according to manufacturer's protocol, and processed for immunoprecipitation after three days as described in the main Methods.

Retroviral production. To produce VSV-G pseudo-typed replication-defective retroviruses, 30 µg of pCLEG plasmids and 35 µg of pVSV-G plasmids were co-transfected into GP2-293 virion packaging cells in a 15 cm dish using Lipofectamine 2000 (Invitrogen). Supernatant containing the virus was collected 48 hr later, passed through a 0.45 µm filter, concentrated by a Centricon-80 centrifugal filter (Millipore), and stored in aliquots at –80°C before use.

References

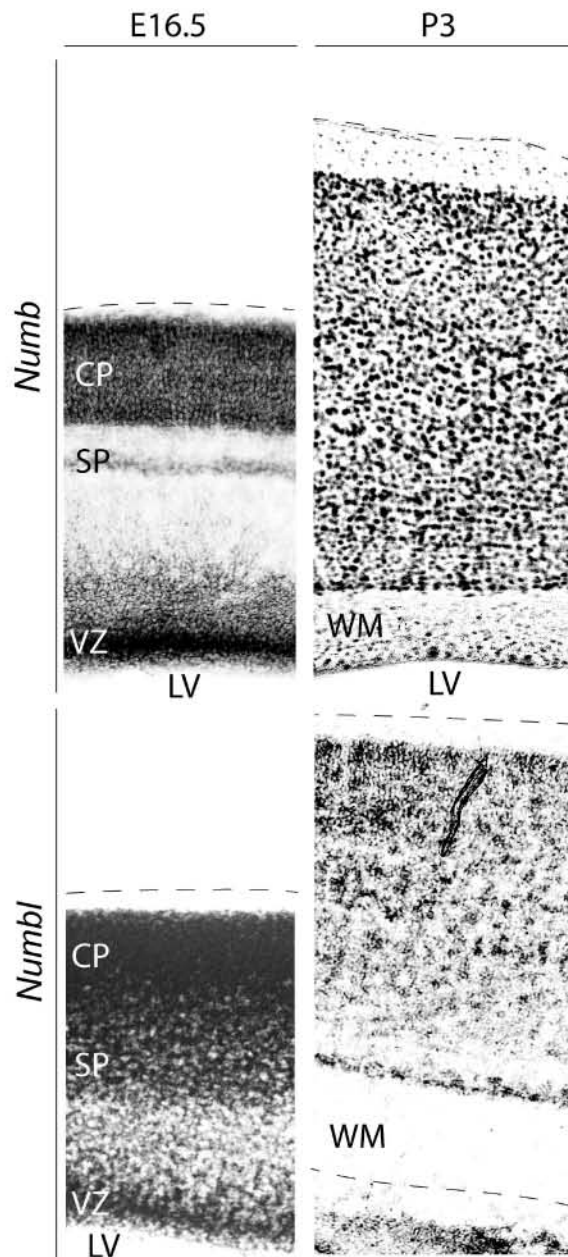
S1. Li, H.S. et al. Inactivation of Numb and Numbl like in embryonic dorsal forebrain impairs neurogenesis and disrupts cortical morphogenesis. *Neuron* **40**, 1105-1118 (2003).

S2. Chen, J.G., Rasin M.R., Kwan K.Y. & Sestan N. Zfp312 is required for subcortical axonal projections and dendritic morphology of deep-layer pyramidal neurons of the cerebral cortex. *Proc. Natl. Acad. Sci. USA* **102**, 17792-17797 (2005).

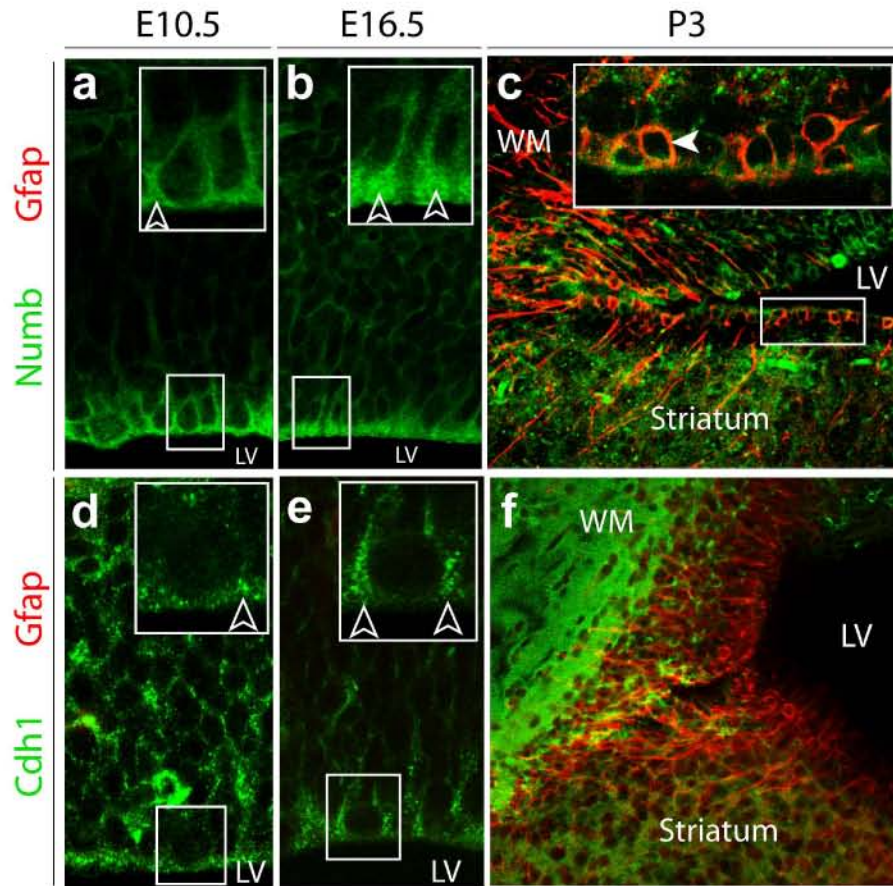
S3. Roncarati, R. et al. The gamma-secretase-generated intracellular domain of β-amyloid precursor protein binds Numb and inhibits Notch signaling. *Proc. Natl. Acad. Sci. USA* **99**, 7102-7107 (2002).

S4. Zhong, W., Feder, J.N., Jiang, M.M., Jan, L.Y. & Jan, Y.N. Asymmetric localization of a mammalian numb homolog during mouse cortical neurogenesis. *Neuron* **17**, 43-53 (1996).

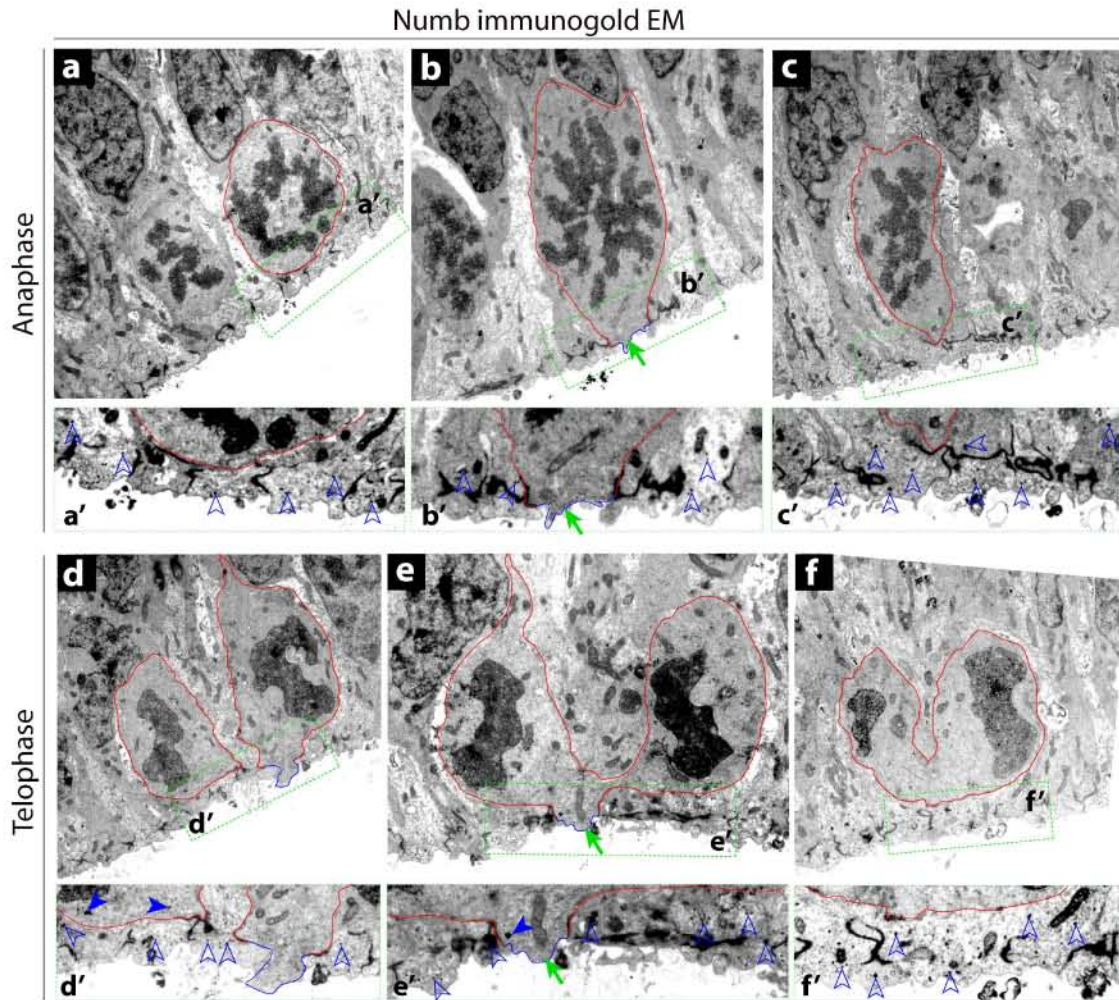
S5. Zhong, W., Jiang, M.M., Weinmaster, G., Jan, L.Y. & Jan, Y.N. Differential expression of mammalian Numb, Numbl like and Notch1 suggests distinct roles during mouse cortical neurogenesis. *Development* **124**, 1887-1897 (1997).



Supplementary Fig. 1 *Numb* and *Numbl* expression in the developing neocortical wall. *In situ* hybridization histochemistry for *Numb* and *Numbl* mRNA at E16.5 and P3. At E16.5, *Numb* and *Numbl* expression is enriched in postmitotic neurons of cortical plate (CP) and subplate (SP), and in progenitor cells of the ventricular zone (VZ). At P3, both genes are expressed in postmitotic cells of all neocortical layers but only *Numb* transcripts can be detected at appreciable levels in the white matter (WM) and in the ependymal lining of the lateral ventricles (LV).

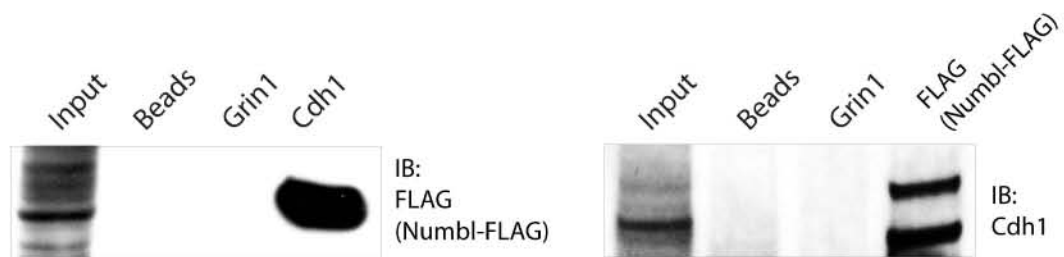


Supplementary Fig. 2 Numb and Cdh1 immunofluorescent staining of the neocortical wall. **(a-c)** Double-immunostaining for Numb (green) and glial fibrillary acidic protein (Gfap; red). At E10.5 and E16.5, Numb is enriched in apical end-feet (open arrowheads) of RGCs. At P3, Numb expression is retained in Gfap⁺ RGCs (arrowhead) of the corticostriatal junction. **(d-f)** Double-immunostaining of the cerebral wall for Cdh1 (green) and Gfap (red). Cdh1 is enriched in apical end-feet (open arrowheads) of E10.5 and E16.5 RGCs and in Gfap⁺ RGCs at P3. Boxes denote areas enlarged within insets. WM, white matter; LV, lateral ventricle.

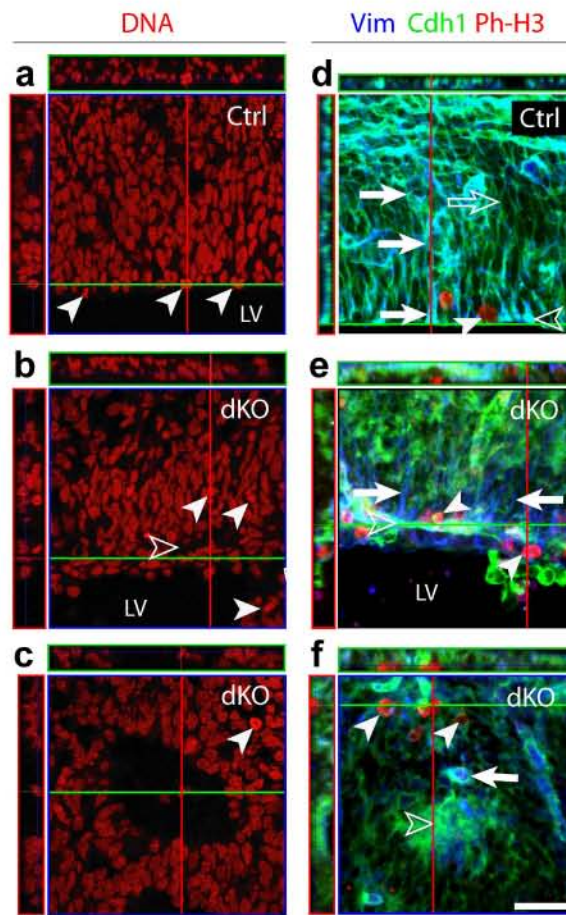


Supplementary Fig. 3 Serial Numb immunogold electron microscopic (EM) analysis of E16.5 mitotic RGCs and surrounding apical end-feet of interphase cells. Representative images from a series of electron micrographs of anaphase (**a-c**) and telophase cells (**d-f**) among E16.5 RGCs immunolabeled for Numb with gold particles. Small panels below anaphase (**a'-c'**) and late telophase cells (**d'-f'**) are enlargements of boxes in **a-c** and **d-f**, respectively. Middle panels show EM images taken at the level of apical membrane (blue outline) of mitotic cells. The basolateral membrane of mitotic cells is outlined in red. Numb is present along the basolateral cytoplasm (arrowheads) and is predominantly absent from the apical membrane of both anaphase and telophase mitotic RGCs (green arrow). However, the majority of gold particles localize to the apical end-feet of adjacent interphase RGCs (open arrowheads). Interphase RGCs surround mitotic cells, extending their end-feet between the mitotic cell body and the lateral ventricle. These thin end-feet extensions can be misinterpreted as the apical cortex of mitotic cells at the light microscopic level. However, as shown here on multiple EM levels, Numb is clearly absent from the apical membrane and present at lower levels along the basolateral membrane of mitotic cells.

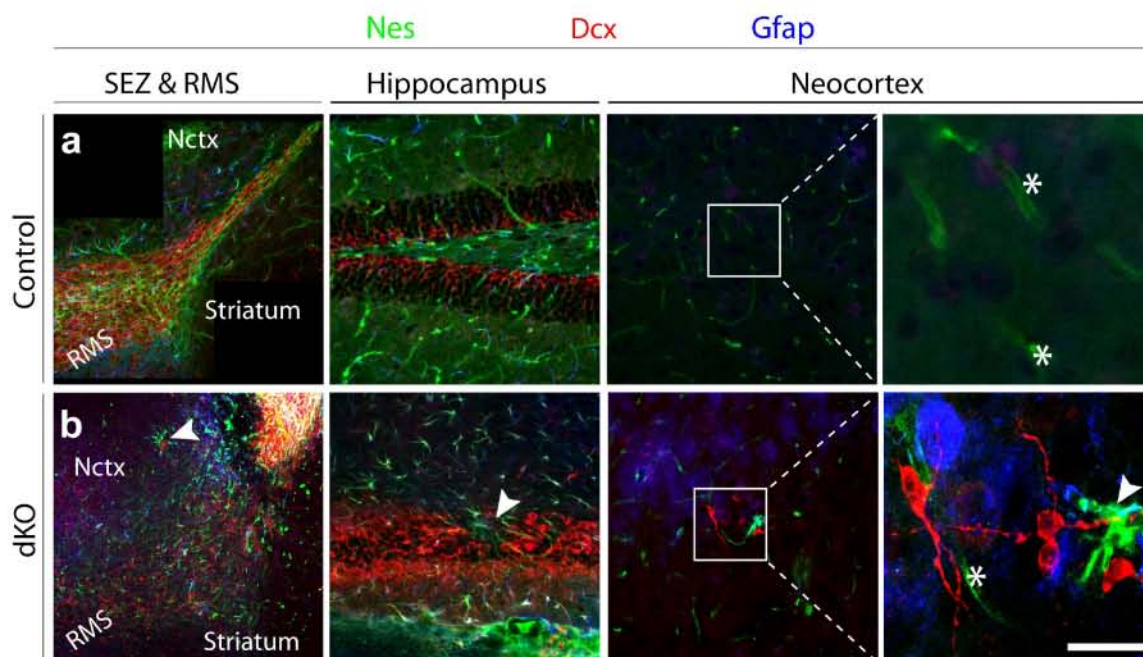
Figure S4, Rasin et al.



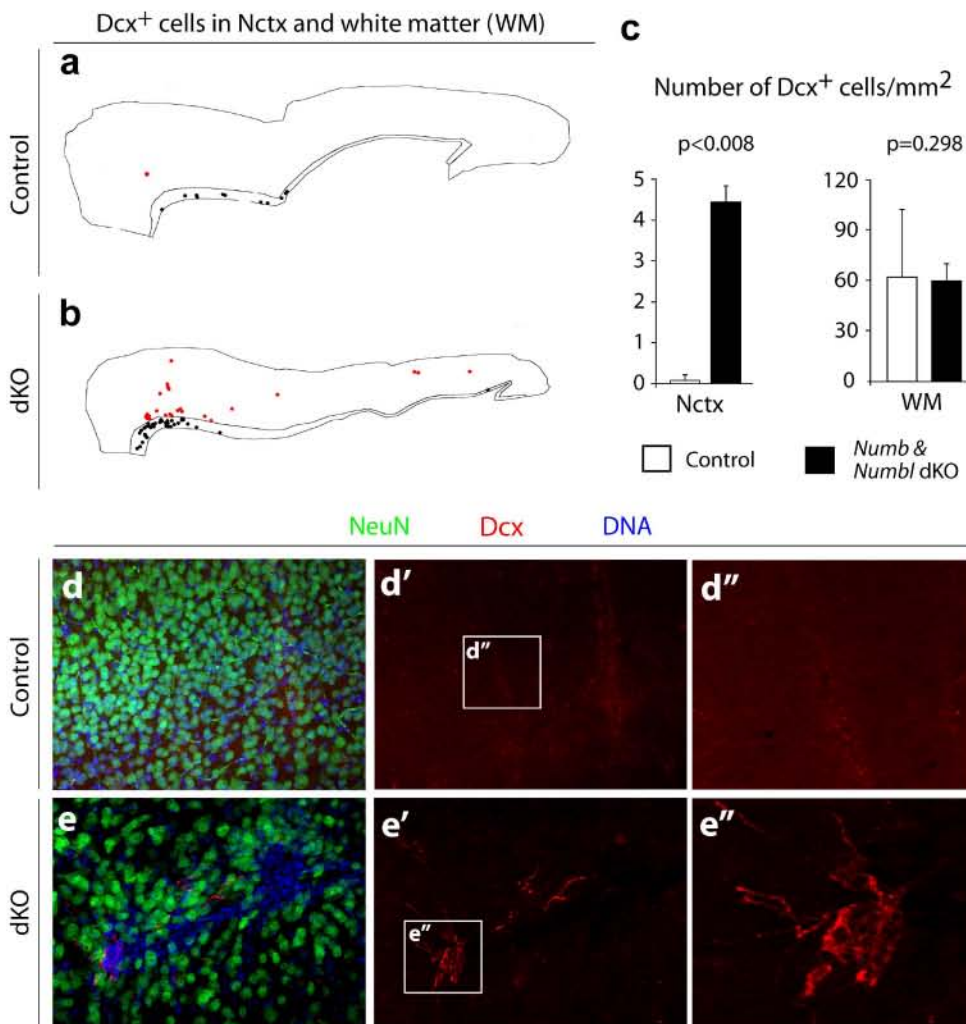
Supplementary Fig. 4 Numbl interacts with Cdh1 in C6-R radial glia-like cells. Immunoprecipitation from the C6-R radial glia-like cell line co-expressing pNumbl-FLAG and pCDH1. Anti-FLAG antibody precipitates Cdh1 and anti-Cdh1 antibody precipitates FLAG-tagged Numbl. Immunoprecipitation was not obtained with control anti-Grin1 antibody when immunoblotted with either anti-Cdh1 or anti-FLAG. IB, immunoblotting antibody.



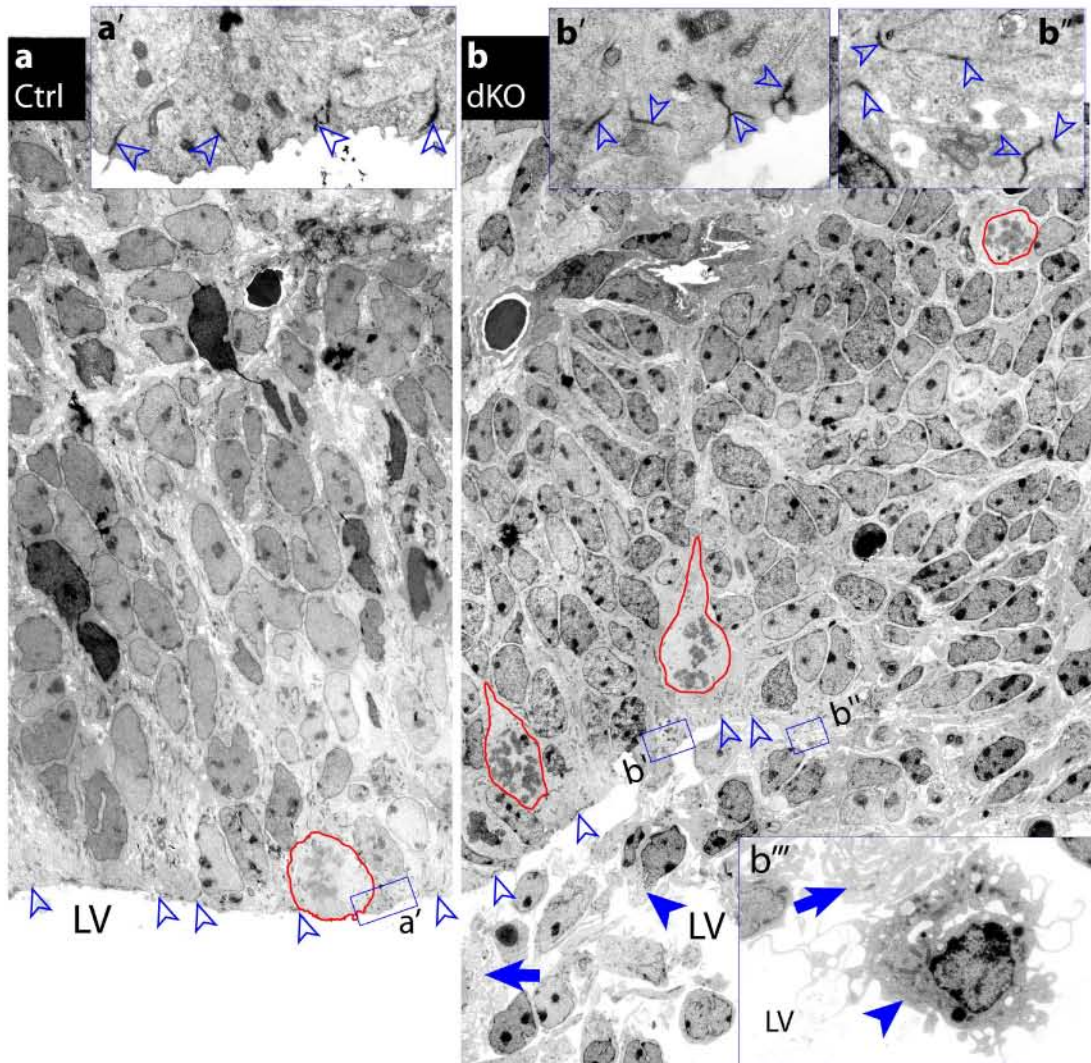
Supplementary Fig. 5 Disruption of neuroepithelial organization and progenitor dispersion in *Numb* and *Numbl* dKO embryos. **(a-c)** Confocal images of dorsal cerebral wall of E16.5 control (Ctrl) and dKO littermates stained for nuclear DNA with propidium iodide (red). **(a)** In Ctrl embryos, nuclei are radially organized with mitotic figures present mainly at the surface of the pseudo-layered VZ (arrowheads). **(b,c)** In the anterior VZ of dKO littermates, cells lose radial organization and gain a cell sparse zone (open arrowhead) near the apical surface. Mitotic figures (white arrowheads) are distributed throughout the disrupted VZ and within cellular clusters in the lumen of the LV. A rosette formation containing mitotic figures (arrowhead) is present in the posterior cerebral wall **(c)**. **(d-f)** Confocal images of E16.5 Ctrl and dKO littermates triple-immunostained for vimentin (Vim; blue), Cdh1 (green) and Ph-H3 (red). **(d)** In Ctrl RGCs, Vim⁺ (blue) radial/basal fibers (arrows) are radially organized and oriented toward the pial surface and span the neocortical wall. Ph-H3⁺ (red) mitotic cells (arrowhead) are present mainly near the VZ surface. Cdh1 is present along the basolateral membrane (open arrows) and end-feet (open arrowhead) resembling the normal honeycomb pattern. **(e,f)** In dKO, Vim⁺ RGCs lose polarity and VZ attachment, and their processes are disorganized **(e,f, arrows)**. Ph-H3⁺ cells (arrowheads) are distributed throughout the disrupted anterior VZ **(e, arrowheads)** and posterior cerebral wall **(f, arrowheads)**. Cdh1 immunostaining is diffuse throughout the VZ, lacking a honeycomb pattern, and ectopically accumulates in cell sparse zones **(e, open arrowhead)**. In the posterior cerebral wall of the dKO, Cdh1 accumulates in the central domain of rosettes **(f, open arrowhead)**. Scale bar: 25 μ m.



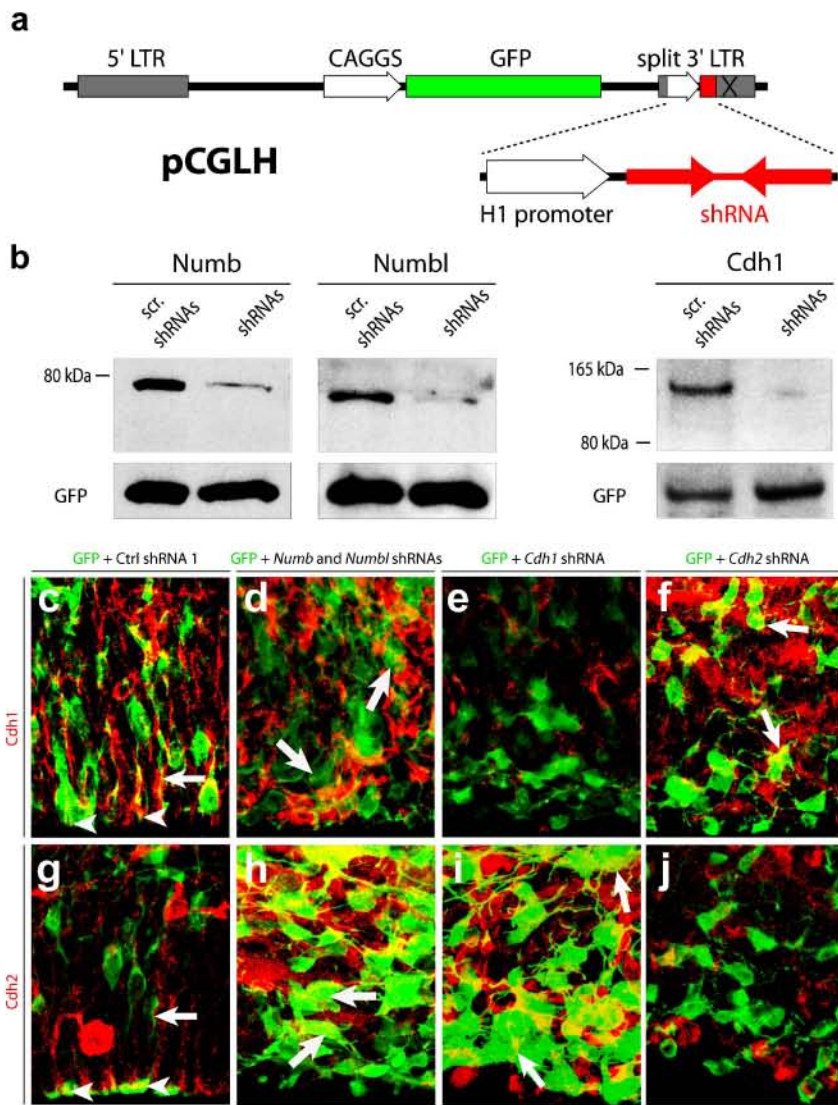
Supplementary Fig. 6 Disorganization of postnatal neurogenic sites and ectopic putative neuronal progenitors in the neocortex of P21 *Numb* and *Numbl* dKO mice. **(a,b)** Triple-immunostaining for nestin (Nes; green), doublecortin (Dcx; red) and Gfap (blue) in P21 control and *Numb* and *Numbl* dKO forebrain. We analyzed dKOs at early postnatal stages (data not shown for P3 and P10) to minimize potential secondary effects of hydrocephalus. **(a)** Control (Ctrl) mice show a normal, compact rostral migratory stream (RMS) composed of Nes⁺/Gfap⁺ progenitors and subependymal zone (SEZ)-derived Dcx⁺ neuroblasts migrating towards the olfactory bulb. In the hippocampal subgranular zone (SGZ), both radial glia-like Nestin⁺/Gfap⁺ progenitors and Dcx⁺ neuroblasts are present and show normal arrangement. Nes⁺ progenitors and Dcx⁺ neuroblasts are not present in the neocortex (Nctx). **(b)** The RMS is dramatically disrupted in dKO littermates, with Nes⁺ progenitors and Dcx⁺ neuroblasts losing cohesion and chain-like arrangement, and deviating from their normal migratory route. Similarly, the hippocampal dentate gyrus lacks one blade, and SGZ-derived radial glia-like progenitors and Dcx⁺ neuroblasts are disorganized. The neocortex and hippocampus of dKO littermates contains numerous rosette-like formations containing clusters of multipolar Nes⁺/Gfap⁺ putative progenitors (arrowheads) surrounded by Dcx⁺ neurons apparently in different stages of maturation. Most Dcx⁺ cells exhibited immature morphologies consistent with newly generated neurons. Detailed analysis revealed that presumptive Nes⁺ progenitors and newly generated Dcx⁺ neurons were clustered adjacent to blood vessels.



Supplementary Fig. 7 Ectopic Dcx⁺ immature neurons in the postnatal neocortex of *Numb* and *Numbl* dKO mice. **(a,b)** Representative NeuroLucida reconstructions and quantification of Dcx⁺ cells in neocortex (Nctx, red dots) and neocortical white matter (WM, black dots) at P21. In Nctx of P21 Control mice, only three Dcx⁺ neurons are present in twelve 60 μ m-thick sagittal tissue sections, and two of them are within close proximity of the white matter. Almost all other neocortical areas are devoid of Dcx⁺ neurons. In the dKO Nctx, clusters of Dcx⁺ cells are present in and around rosettes. These cells have leading processes oriented randomly and display a migratory phenotype. The distribution of Dcx⁺ cells is quantified in **c**. **(d,e)** Representative fluorescent images of P21 telencephalon immunostained for NeuN (green) and Dcx (red). **(d)** In Controls, most neurons in neocortical areas express NeuN, a marker of mature neurons **(d)**, but lack immature Dcx⁺ neurons **(d',d'')**. **(e)** In the dKO neocortex numerous clusters of Dcx⁺ cells are often found in and around the rosette-like formations characteristic of this mutant. Leading processes of these cells were pointed randomly, displayed a migratory phenotype, and were rarely immunolabeled with NeuN antibody **(e)** indicating that they are predominantly immature neurons.

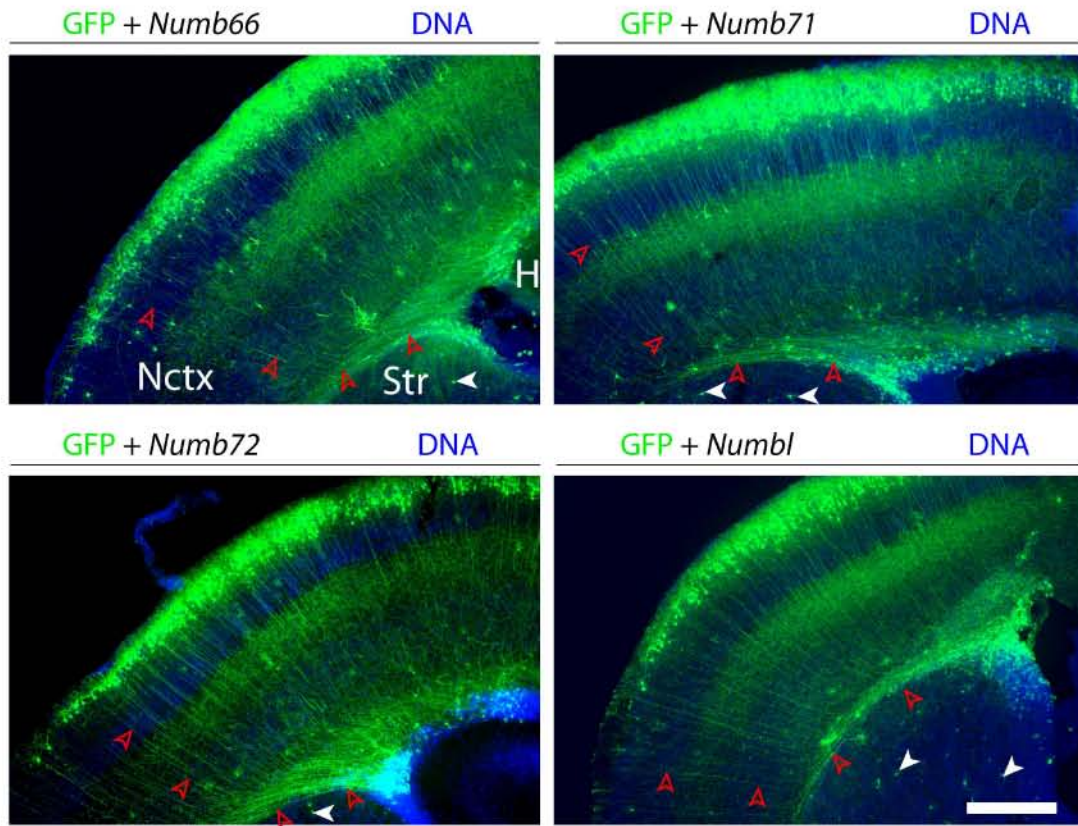


Supplementary Fig. 8 Disorganized adherens junctions and RGC alignment in the ventricular zone of E16.5 *Numb* and *Numbl* dKO embryos. **(a)** In E16.5 Ctrl embryos, highly polarized interphase RGCs have radially-oriented oval nuclei distributed at different levels of VZ forming a columnar pseudo-stratified layer. Round mitotic cells (outlined in red) are mainly present near the VZ surface. Adherens junctions (**a,a'**, open arrowheads) appear as electron-dense contacts on the apical processes of neighboring interphase RGCs. **(b)** In E16.5 dKO littermates, the VZ is less columnar with disorganized surface alignment. Many mitotic cells are abnormally dispersed throughout the VZ. The remaining adherens junctions exhibit decreased electron density and abnormal organization (**b,b',b''**, open arrowheads). Multipolar cells (**b,b'''**, arrowhead) and multiple processes (**b,b'''**, arrows) are present at the VZ surface and within the LV. Boxes denote areas enlarged in insets. LV, lateral ventricle.

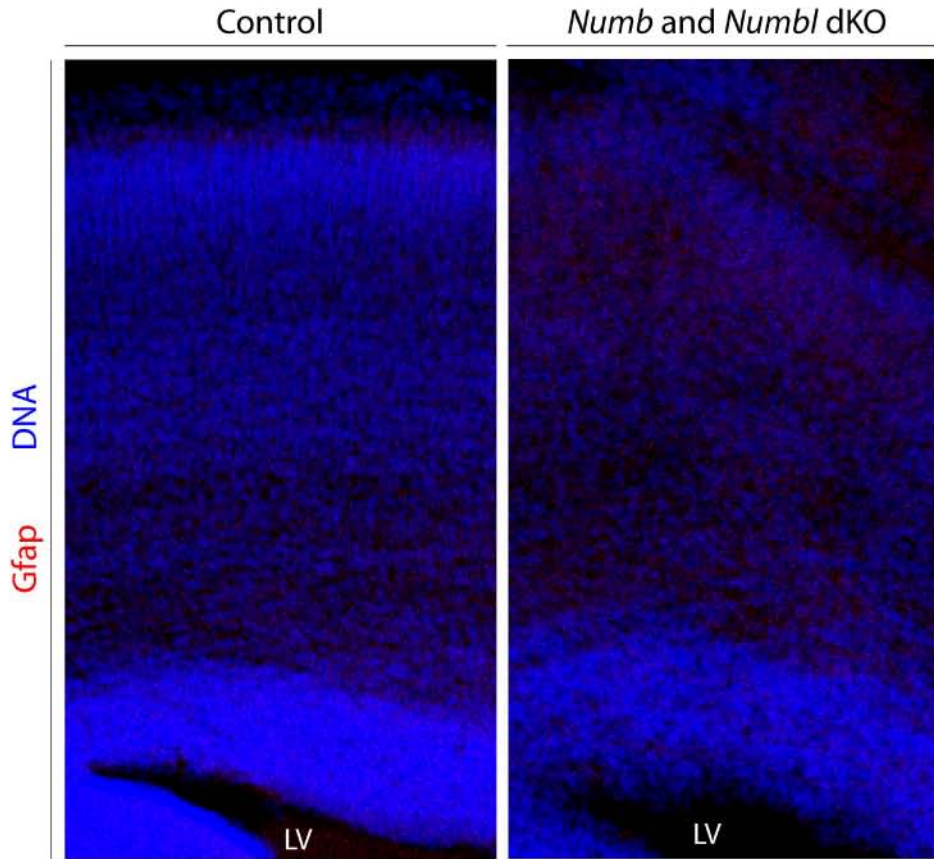


Supplementary Fig. 9 Knocking down *Numb*, *Numbl*, *Cdh1* and *Cdh2* with shRNAs. **(a)** Design of pCGLH RNAi vector. **(b)** Western blots show shRNA-mediated reduction of *Numb*, *Numbl* and *Cdh1* in N2a cells. ShRNA sequences are listed in Supplementary Table 2. *Cdh2* levels in N2a cells were below our threshold of detection (data not shown). **(c-j)** E16.5 GFP⁺ VZ cells electroporated with pCGLH plasmids at E13.5. **(c,g)** VZ cells expressing control (Ctrl) shRNAs exhibit an elongated bipolar morphology with the apical end feet at the VZ surface. *Cdh1* and *Cdh2* are present at the membrane (arrow) and apical end-feet (arrowheads). **(d,h)** VZ cells co-expressing *Numb* and *Numbl* shRNAs and GFP (green) lack typical RGC morphology. *Cdh1* (**d**, red) and *Cdh2* (**h**, red) are localized throughout the cytoplasm of GFP⁺ cells (**d,h**, arrows). **(e,i)** VZ cells expressing *Cdh1* shRNAs and GFP (green) also lack typical RGC morphology, similar to the result of silencing *Numb* and *Numbl*. GFP⁺ cells have significantly reduced *Cdh1* expression but localize *Cdh2* (**i**) at the membrane contacts of *Cdh1* shRNA expressing cells. **(f,j)** VZ cells expressing *Cdh2* shRNAs and GFP (green) display similarities to the abnormal *Numb* and *Numbl* and *Cdh1* knock-down phenotypes. These GFP⁺ cells do not express *Cdh2*, but *Cdh1* is present at cellular membrane contacts of *Cdh2* shRNA expressing cells (**f**, arrows).

Figure S10, Rasin et al.



Supplementary Fig. 10 Forced expression of all Numb isoforms and Numb1 promotes radial polarity after the end of neocortical neurogenesis *in vivo*. Epifluorescent images of P10 brains electroporated *in utero* at E16 with pCLEG plasmids expressing one of three isoforms of mouse Numb or Numb1. In all cases, GFP⁺ cell bodies were present in the upper layers of the neocortex (Nctx) and striatum (Str, white arrowheads) as post-migratory neurons, and in the subependymal zone (SEZ) of the cortico-striatal junction. GFP⁺ cells in the SEZ have radial processes either spanning the entire thickness of the neocortex (red arrowheads) or extending deep into the Str. H, hippocampus. Scale bar: 500 μ m.



Supplementary Fig. 11 Astroglial differentiation does not occur prematurely in late *Numb* and *Numbl* dKO embryos. Representative confocal images from the frontal neocortical wall of control and *Numb* and *Numbl* dKO littermates at E18.5, immunostained for Gfap (red). Gfap immunopositive astrocytes were largely absent from the neocortical wall. DNA staining, shown in blue, highlights the disruption of cortical lamination and lining integrity of the lateral ventricle (LV) in *Numb* and *Numbl* dKO.

| Protein/Marker | Host | Dilutions | Source/Catalog No. | Immunogen | Description and notes |
|---|------------|-----------------------------|-------------------------------|--|--|
| Bcl11b (also known as Ctip2) | Rat | 1:100 (IHC) | Abcam/ab18465 | Human fusion protein (a.a. 1-150) | Transcription factor in layers V and VI pyramidal neurons |
| Cadherin 1 (Cdh1; also known as E-cadherin) | Mouse | 1:100 (IHC); 1:500 (WB) | BD Transduction Labs/610181 | Synthetic peptide (a.a. 735-883) | Cell adhesion protein on the basolateral membrane |
| Cadherin 1 (Cdh1) | Mouse | 1:100 (IHC); 1:500 (WB) | BD Transduction Labs/6101405 | Synthetic peptide (a.a. 735-883) | Cell adhesion protein on the basolateral membrane |
| Cadherin 1 (Cdh1) | Rat | 1:100 (IHC) | Abcam/ab8993 | MCF-7/AZ cells expressing Cdh1 | Cell adhesion protein on the basolateral membrane |
| Cadherin 2 (Cdh2; also known as N-cadherin) | Mouse | 1:100(IHC); 1:500 (IP, WB) | Zymed/18-0224 | Intracellular domain of chicken Cdh2 (N-Cadherin) | Cell adhesion protein on the basolateral membrane |
| Catenin, alpha 1 (Cttna1; alpha(E)-catenin) | Mouse | 1:100 (IHC); 1:500 (IP, WB) | BD Transduction Labs/610194 | C-terminus of mouse Cttna1 | Cadherin associated protein |
| Catenin, beta 1 (Cttnb1) | Mouse | 1:100 (IHC); 1:500 (IP, WB) | BD Transduction Labs/610154 | C-terminus of mouse Cttnb1 | Cadherin associated protein |
| Cut-like 1 (Cutl1; also known as Cux1) | Goat | 1:100 (IHC) | Santa Cruz Biotech/sc-6327 | C-terminus of mouse Cut1 | Transcription factor in layers II-IV pyramidal neurons |
| Doublecortin (Dcx) | Goat | 1:500 (IHC) | Santa Cruz Biotech/sc-8066 | C-terminus of mouse Dcx | Microtubule-associated protein in migrating neurons |
| FLAG | Rabbit | 1:1000 (WB) | Sigma/F7425 | Synthetic FLAG sequence (DYKDDDDK-GC) | Epitope for protein tagging |
| Forkhead box P2 (Foxp2) | Goat | 1:750 (IHC) | Abcam/ab1307 | Synthetic peptide (REIEEPLSEDL) | Transcription factor in layers V and VI pyramidal neurons |
| Forkhead box P2 (Foxp2) | Rabbit | 1:500 (IHC) | Sestan Lab | Synthetic peptide (GNSSPGCSPPQPHHS) | Transcription factor in layers V and VI pyramidal neurons |
| Glial fibrillary acidic protein (Gfap) | Guinea Pig | 1:500 (IHC) | Advanced Immunoch/31223 | GFAP purified from human brain | Intermediate filament protein in astrocyte |
| Green fluorescent protein (GFP) | Rabbit | 1:3000 (IHC, WB) | Molecular Probes/A-11122 | Green fluorescent protein | |
| Nestin (Nes) | Mouse | 1:75 (IHC) | Chemicon/MAB5326 | Nestin purified from embryonic rat spinal cord | Intermediate filament protein in neuroepithelial and RGCs |
| Neuronal Nuclei (NeuN) | Mouse | 1:1000 (IHC) | Chemicon/MAB377 | Purified cell nuclei from mouse brain | Neuron specific nuclear marker |
| N-methyl D-aspartate 1 (Gri1) | Rabbit | 1:200 (IHC); 1:100 (IP) | Chemicon/AB1516 | Synth. peptide (LQNKDVTLPRAIEREEGQLQLCSRHRES) | Glutamate membrane receptor |
| Numb | Goat | 1:100 (IHC); 1:500 (IP, WB) | Abcam/ab4147 | Synthetic peptide (PFSSDLQKTFEIEL) | |
| Numb | Rabbit | 1:500 (IHC, WB); 1:200 (IP) | Zhong et al., 1998 | Synthetic peptide (a.a. 489-522) | |
| Numb | Rabbit | 1:275 (IHC) | Upstate/07-147 | Synthetic peptide (C-TTHPHQSPSLAKQQTFPPQE) | |
| Phospho-Histone H3 (Ph-H3) | Rabbit | 1:1000 (IHC) | Upstate/06-570 | Synthetic phosphopeptide (ARKpSTGGKAPRKQLC) | Histone protein phosphorylated during mitosis |
| Phosphorylated Vimentin (Ph-Vim) | Mouse | 1:50 (IHC) | Kamei et al., 1998 | Synthetic phosphopeptide (SLYSSpSPGGAYC) | Intermediate filament protein phosphorylated in mitotic RGCs |
| Prominin 1 (Prom1; CD133) | Rat | 1:100 (IHC) | eBioscience/14-1331 | E12 mouse telencephalon, clone 13A4 | Microvilli-specific protein on the apical plasma membrane |
| Rab11 | Rabbit | 1:100 (IHC) | Santa Cruz Biotech/sc-9020 | Human RAB11 (a.a. 130-216) | Small GTPase in recycling endosomes |
| SMI32 | Mouse | 1:1000 (IHC) | Sternberger Monoclonals/SMI32 | Non-phosphorylated epitopes in neurofilament H | Neurofilament protein in layers III and V pyramidal neurons |
| TuJ1 | Mouse | 1:1000 (IHC) | Covance/MMS-435P | Microtubules derived from rat brain (epitope CEAQGPK) | Neuron specific class III β -tubulin |
| Vimentin | Mouse | 1:250 (IHC) | Chemicon/MAB1661 | Vimentin from human mesenchymal cells and derived sarcomas | Cytoskeletal protein |

| Name | Source or shRNA sequences (5' to 3') | Insert size or position | Vector |
|------------------------|---|--------------------------------------|-------------|
| CLEG | Chen et al., 2005 | | pCLEG |
| CYLH | | | pCYLH |
| CGLH | | | pCGLH |
| CAGGS-GFP | Gift from Jun-ichi Miyazaki (Osaka University) | | pCAGGS |
| Numb65-FLAG | Roncarati et al., 2002 | Mouse Numb65 | pcDNA3-FLAG |
| Numb1-FLAG | Roncarati et al., 2002 | Mouse Numb1 | pcDNA3-FLAG |
| CLEG-hNICD | | Intracellular domain of human NOTCH1 | pCLEG |
| CLEG-Numb65 | | Mouse Numb65 | pCLEG |
| CLEG-Numb66 | | Mouse Numb66 | pCLEG |
| CLEG-Numb71 | | Mouse Numb71 | pCLEG |
| CLEG-Numb72 | | Mouse Numb72 | pCLEG |
| CLEG-Numb1 | | Mouse Numb1 | pCLEG |
| CDH1 | Gift from Cara Gottardi (Northwestern University) | Human CADHERIN 1 | pcDNA3 |
| CDH2 | Origene/ Cat # TC119018 | Human CADHERIN 2 | pCMV |
| Numb shRNA-1 | CCACTTTCACAAGAGAAGG | | pCYLH |
| Numb shRNA -2 | GCCGAAAGAGAGGAGATCA | | pCYLH |
| Numb1 shRNA-1 | GGCACCATGAACAAGTTAC | | pCYLH |
| Numb1 shRNA-2 | GGTGCCTTCTGTGCTCCT | | pCYLH |
| Cdh1 shRNA-1 | GCAGCAATACATCCTTCAT | | pCGLH |
| Cdh1 shRNA-2 | GGACTTAGAGATTGGCGAA | | pCGLH |
| Cdh2 shRNA-1 | CAGGTCTGATAGAGATAAA | | pCGLH |
| Cdh2 shRNA-2 | GAACGAAACAACCAGATTA | | pCGLH |
| Control (Ctrl) shRNA-1 | GCAGGAATGCAGCGTTCAT | | pCGLH |
| Control (Ctrl) shRNA-2 | GGCAGCATCATCATGTTAC | | pCYLH |
| Control (Ctrl) shRNA-3 | GGTGACCATCACTGCACCT | | pCYLH |
| Control (Ctrl) shRNA-4 | ATCAAGCACGTGAATCGCA | | pCYLH |
| Control (Ctrl) shRNA-5 | AGAGCAAGCATGCGAGAAG | | pCYLH |

Supplementary Table 2 Plasmids and shRNA sequences used in this study.